8 Imaging Mass Spectrometry

ALEXANDRA VAN REMOORTERE, EMRYS A. JONES, ANDRÉ M. DEELDER, and LIAM A. MCDONNELL

Department of Parasitology, Leiden University Medical Center, Leiden, The Netherlands

8.1 INTRODUCTION

Molecular imaging is one of the cornerstones of the experimental methods available for understanding the spatial complexity of biological tissues and cells. Ideally, imaging methods should provide detailed information of a number of tissue components and provide a resolution that surpasses that of individual cells. Most current methodologies often require *a priori* knowledge of the molecules of interest. Microscopy has long been one of the most powerful techniques to study the distribution of biologically relevant compounds in tissues. Immunohistochemical methods were first studied in 1942 in the work of Coons *et al*. [1]. They presented a method employing the specificity of an antibody labeled with fluorescein for the localization of antigens under a fluorescence microscope. It was a generic method for the histological localization of any antigen of interest. The antibody could be conjugated with simple chemical compounds without destroying its capacity to react with the antigen. One of the limitations of immunohistochemistry is that simultaneous visualization of different antigens can be very challenging and posttranslational modifications of proteins can be difficult to detect because of the lack of an available antibody specific for these modifications.

The ability of modern proteomic techniques to identify and quantify the levels of up to thousands of proteins from a tissue or biofluid sample has transformed medical and biological research. In addition to global protein profiling [2], methods have been developed that target protein isoforms [3,4] or their interactions [5], specific pathological entities [6], or subcellular components [7]. It has been increasingly recognized how the rich molecular information provided by this array of approaches offers new possibilities in the clinical field. This ranges from new insights into the molecular changes associated with pathogenesis, the identification of new therapeutic targets, to improved diagnosis

Encyclopedia of Drug Metabolism and Interactions, 6-Volume Set, First Edition.
Edited by Alexander V. Lyubimov.

and prognosis through the determination of biomarker proteins and protein profiles associated with a disease and its progression [8]. Many clinical institutions have initiated research programs for the identification of disease biomarker proteins and protein profiles, mostly in easily accessible body fluids such as plasma, serum, and urine.

Difficulties associated with sample volume and complexity, dilution of the biomarkers, and the intrinsic variability of the protein content of body fluids have led to the alternative strategy of searching for biomarkers in the affected tissue. Recent notable examples include a combination of tissue microdissection, protein extraction, and extensive peptide/protein separation to quantitatively investigate the changes in protein content associated with the different stages of diseases [6,8].

Several groups have demonstrated how mass spectrometry (MS)-based methods can be directly applied to tissue. Rapid progress in the field now allows the parallel analysis of 100–200 proteins, high sensitivity and selectivity, and the ability to distinguish between close variants [9–11]. Histology-directed tissue profiling, in which localized MS is used to generate peptide and protein signatures of specific regions of a tissue previously annotated by a pathologist, has demonstrated how the signatures of the different regions can be used to classify the tissue [12,13]. These classifications, based on the nontargeted analysis of the peptides and proteins present in specific regions of the tissue, demonstrate the ability of this technique to acquire clinically relevant data. The candidate markers determined by these classifications are based on the levels of many peptides and proteins and provide an example of a general observation in biomarker research, namely, that a single protein biomarker may not be sufficient to annotate the complexity of real biological systems [14,15]. Protein profiling by imaging MS has been performed on human brain tumors [11,16,17], rat pituitary [18], mouse brain [19], mouse prostate [10], mouse epididymis [9], and in animal models for neurological disorders including Parkinson's disease [20] and Alzheimer's disease (AD) [21].

Imaging MS can be considered a spatially resolved direct tissue analysis and uses the same tools to simultaneously analyze the distribution of 100–200 proteins in tissue and to associate the differential protein images with histopathological analysis. Several studies have already shown how imaging MS can be used to chart the variation in protein content in pathological tissues and revealed that changes in distribution and biochemical content are widespread [22]. The spatiochemical information obtained directly from the tissue (thus not diluted by body fluids) and without prior knowledge of the sample's biomolecular content has great potential as a discovery tool to identify those changes associated with a specific diagnosis/prognosis. In many regards, it is the aim of imaging MS to become a peptide/protein screening that complements histopathological analysis.

Imaging MS comprises the collection of a mass spectrum at each of a regular series of points across the tissue section. Using these spectra, it is possible to plot the relative intensity of the individual m/z peaks in the mass spectrum across the tissue section, visualizing the distribution of the individual molecular ions. A two-dimensional map can be generated for each mass peak of interest in the mass spectrum and depicted as an intensity or pseudocolor heat map. Reproducible sample preparation, mass spectral acquisition, and data processing allow these maps to be compared between related samples to assess which biomolecular changes are associated with disease (and its progression). In current experimental workflows, the imaging MS analysis is aligned with an optical image of the tissue section (H&E stained after the imaging MS experiment) [23,24]. This allows the direct comparison of the specific biomolecules with the tissue's

morphology or the determination of the molecular content of histological regions of interest. Advanced data-analysis tools enable the data sets to be interrogated to reveal which peptides and proteins have similar profiles [25–27], which are correlated with specific histological features [27] and can be used to classify the tumor type of the tissue [27,28].

One main advantage is its lack of *a priori* knowledge since any compound of interest at the surface of the sample can potentially be detected. Imaging MS is very useful as a discovery tool where a tissue section can be investigated without knowing in advance what specific proteins have changed in a comparative study. Furthermore, imaging MS also allows the detection of posttranslational modifications, given that these generally involve mass changes. Unfortunately, many of the fixation approaches developed for optical and electron microscopy are not suitable for imaging MS, and so new MS-specific protocols have been designed, this is described in the following sections. Imaging MS has a significant potential to be used in a targeted approach as well, such as for monitoring drug delivery and metabolism. Imaging MS can visualize and distinguish the parent drug and its metabolites in contrast to autoradiography as no labeling is required.

While profiling MS of a tissue section can be of interest to analyze discrete regions of a tissue, imaging MS becomes necessary when the focus is the protein distribution information. The analysis of various cell types can be correlated to the tissue architecture, thereby enabling peptides and proteins specific to the tumor and/or adjacent stroma to be identified. High resolution images are desirable when a defined substructure is present; however, they may also be utilized as a discovery tool for a suspected yet otherwise not morphologically detectable transformation such as has been observed for tumor margins [29].

Immunohistochemical methods allow localization of antigens, antibodies, and numerous other cell and tissue components and have facilitated the development of specific diagnostic tests. Imaging MS offers the potential for the simultaneous analysis of many molecular species present in a single biopsy regardless of the availability of specific antibodies. Furthermore molecules spanning multiple molecular classes, which may be involved in a disease state, can be investigated. For clinicians, this will permit molecular assessment of tumor biopsies with the potential to identify subpopulations that are not evident based on the cellular phenotype determined microscopically [30]. In addition, this technology also permits imaging the distribution of low molecular weight compounds such as lipids, drugs, and metabolites, opening new possibilities for the measurement of concomitant protein changes in specific tissues after systemic drug administration.

Imaging MS has been used in a wide variety of applications since its development by Caprioli *et al*. in 1997 [18]. Improvements have been made in sample handling, spatial resolution, sensitivity, robustness, speed, and instrumentation, and molecular images up to a resolution of 5 μm can now be acquired. Today, imaging MS is applied in different research fields, from fundamental research to clinical applications (cancer research, neuroscience, and pharmaceutical research).

Imaging MS is increasingly used in clinical proteomics as a tool for candidate biomarker discovery. A large range of biomolecules, spanning multiple molecular classes, can be simultaneously analyzed without predefining the molecules of interest (e.g., labeling). This multiplex, nontargeted analysis enables a comparative analysis of the biomolecular content of diseased samples and, as such, may be used to complement

established histopathological practice. However, before imaging MS can be routinely used in a clinical setting, a large number of patient samples need to compared to provide statistical foundation necessary for a new diagnostic tool. Good collaborations with pathologists and surgeons are crucial for ensuring the quality of the samples and the interpretation of the subsequent experimental results.

Designing an imaging MS experiment includes several important aspects that will optimize signal quality. Sample preparation for imaging MS plays a crucial role in generating reproducible quality data, and this is described below.

8.2 METHOD OVERVIEW

The workflow of a typical MALDI (matrix-assisted laser desorption/ionization) imaging MS experiment is given in Fig. 8.1, and all different steps are described in detail in this section. Sample handling, from the point of collection and isolation to the final data acquisition, is one among the most crucial steps in imaging MS for achieving qualitative and reproducible results. Goodwin *et al*. [31] have given a schematic representation of the MALDI imaging MS workflow, with an overview of which factors need to be considered to minimize variation and which factors can be used to optimize performance based on four different key stages (tissue collection, tissue cutting, tissue pretreatment, and matrix application), which we have discussed in the following paragraphs (Fig. 8.2). It is essential to maintain the integrity and spatial localization of the molecules in the original tissue. Since the introduction of imaging MS, many reviews have been published that address sample handling and sample preparation [30,32–37].

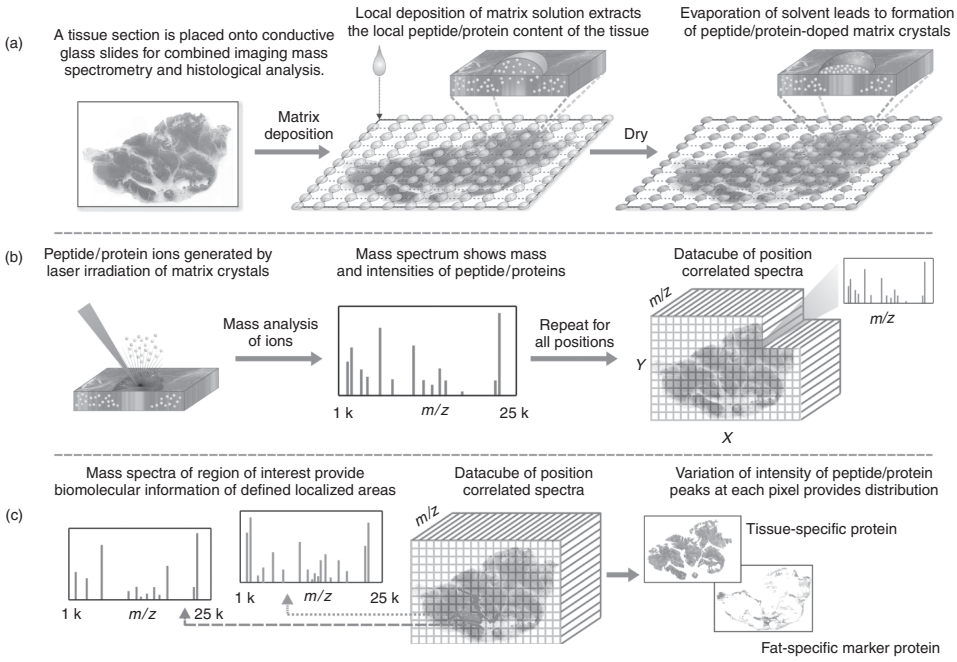

Figure 8.1 Schematic of the MALDI imaging MS workflow.

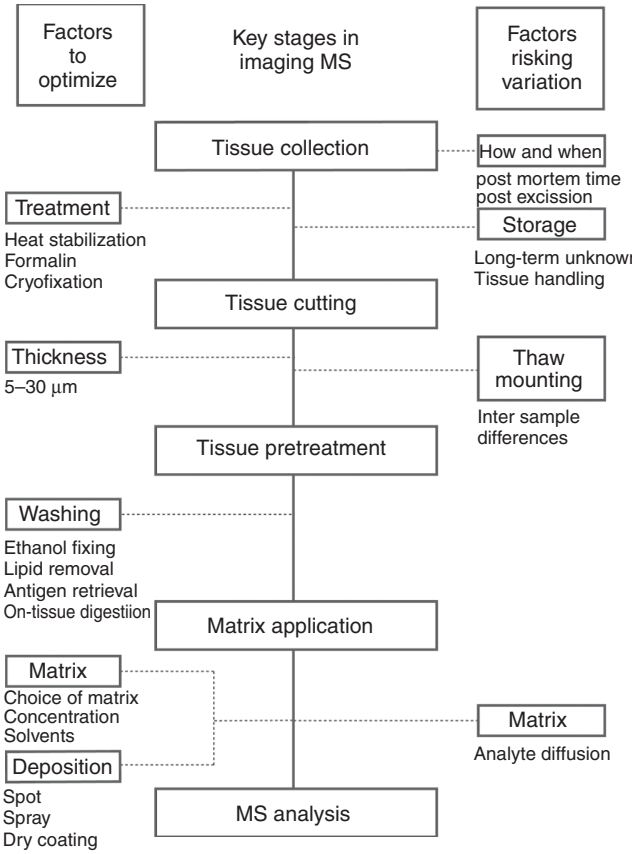

Figure 8.2 MALDI imaging MS workflow and the experimental factors that must be considered to minimize variation and optimize performance. The manual nature of these steps can make them highly prone to user artifacts unless stringent protocols are followed [38].

8.2.1 The Tissue Sample

The integrity of a tissue sample is key to any analysis of its biomolecular content. An imaging MS procedure starts with tissue collection, and this is the first important step toward high quality and reproducible results. Tissue collection must be performed in accordance with the appropriate ethical guidelines. It has been shown that postmortem changes can occur within minutes [31]. Techniques to limit the impact of postmortem degradation suppress enzymatic activity by denaturation of proteins, chemical fixation, or cryofixation. In animal studies, a common condition to preserve tissue morphology as well as the native distribution of biomolecules is that tissues must be rapidly dissected following animal sacrifice and flash-frozen in liquid isopentane or nitrogen. For the collection of tissue specimens derived from humans, standardized protocols and well-documented procedures should be agreed on/consulted with the surgeons and the pathologists. After freezing, tissues should be stored at -80°C.

The majority of the imaging MS studies have been performed on flash-frozen tissue sections, although recent developments have enabled imaging of formalin-fixed paraffin-embedded (FFPE) tissues [39,40]. Formalin fixation stabilizes proteins by

chemical cross-linking, thus preventing postmortem enzymatic proteolysis while maintaining the cellular histology [41]. FFPE tissue blocks are stored at room temperature. The cross-linked proteins are difficult to extract from the tissue with standard matrix application procedures. To circumvent the cross-linking induced by formalin fixation, a protocol based on ethanol fixation [42] or on RCL2/CS100 fixation (a non-cross-linking organic fixative [43]) in combination with paraffin embedding has been developed and proved to be suitable for proteomic analysis and tissue imaging. The advantage of using FFPE tissues for imaging MS is the large existing collections of FFPE tissues in hospital tissue banks: The ability to search for biomolecular signatures associated with specific pathological features and known clinical outcomes would represent a powerful tool for clinical biomarker research. However, in order to achieve this goal, it will be necessary to identify which tissues are still suitable for analysis, as the retrospective nature of the tissue banks means that many of the tissues may have been collected and processed using methods less suited to modern bioanalytical techniques.

After freezing, the tissue can be fixed to the cryostat stage using a droplet of water or 10% gelatin. The use of optimal cutting temperature (OCT) embedding media should be avoided as much as possible because this compound includes many water-soluble polyethylene glycol compounds that significantly interfere with the imaging MS experiment [32]. The potential interference from these compounds is such that if one is using a shared cryostat, the cryostat should be comprehensively cleaned before use. When an embedding medium is required for sectioning, 10% gelatin or agarose can be used [44]. The frozen tissues are then sectioned and transferred onto cold indium-tin oxide (ITO)-coated glass slides [45] or other holders suitable for imaging MS experiments. It is important to deposit the section uniformly without scratches [46]. The tissues are normally mounted onto the target plate or glass slide by gently heating the underside of the slide with a finger. Immediately after sectioning, the tissue section should be dried for at least 10 min in a vacuum desiccator to remove residual water from the tissue.

To date, the majority of imaging experiments has been focused on the analysis of thin frozen tissue sections. The sections, 5–50 μm thick, are collected at -5 to -25° C using a cryomicrotome. For each tissue, the cutting temperature may need to be optimized. Thicker sections are easier to collect; however, thinner sections have been shown to provide higher quality mass spectra [47]. When a study is set up, wherein multiple sections are required, it is recommended to collect these sections at the same time to prevent repeated handling of the tissue, although side effects such as oxidation may increase [38].

Goodwin *et al*. [31] showed postmortem degradation in brain tissue section. The intensity of a range of markers was seen to vary when tissue sections were kept on room temperature and on timescales of 30 s to 3 h; while some peptides/proteins were stable, the intensities of several peptides were found either to decrease (degradation) or increase (degradation product) (Fig. 8.3). Furthermore, it was shown that within each of these classes, there is clearly a range of rates at which the markers are observed to change, which could be location dependent. These results indicate that warming a sample for a short period, for example, during sectioning and mounting, may perturb the markers observed, in particular, when human tissue samples retrieved from the hospital are used. To guard against misinterpreting artifacts as real markers, a rigorous sample handling procedure should be employed. Approaches to prevent postmortem degradation have been developed, for example, Denator AB has released the

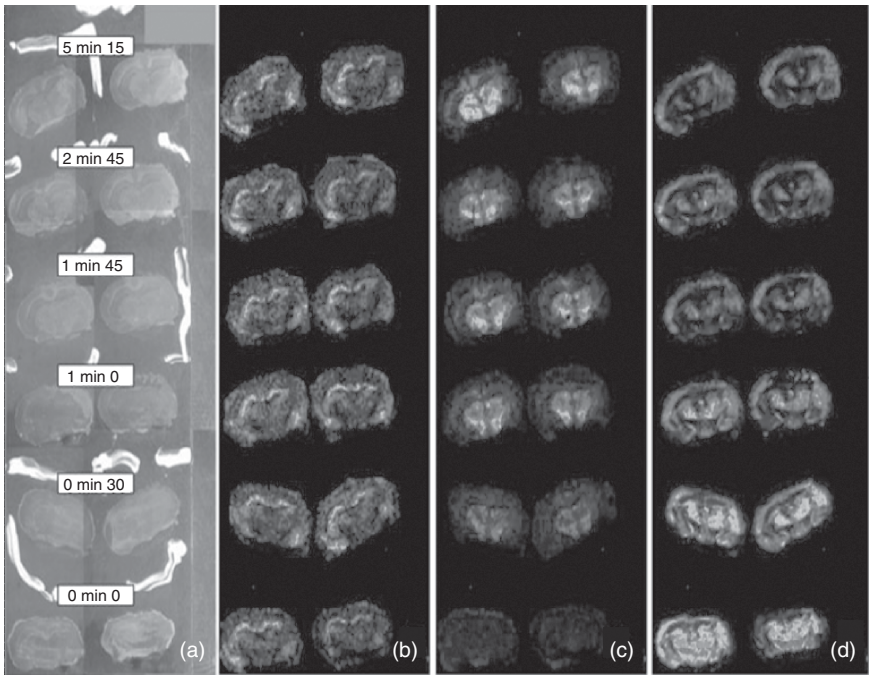

Figure 8.3 Investigation of postmortem degradation in MALDI imaging MS. Optical and MALDI imaging MS analyses of 14-μm-thick mouse brain sections thaw-mounted onto ITO–coated slides. (a) Optical image of the mounted transcoronal sections. Strong white areas are Tipp-Ex™ spots applied to the slide to coregister images. MALDI imaging MS analyses after 0, 0.5, 1, 1.75, 2.75, and 5.25 min for peptide peaks at m/z (b) 2608, (c) 2479, and (d) 6724 [31]. (See color insert.)

tissue stabilization system, Stabilizor T1 (Denator AB, Sweden), that rapidly inactivates enzymes by heat-induced denaturation and reduces postmortem degradation to improve the analysis of fresh and frozen tissue samples [48,49]. In an initial study, it was shown that posttranslational phosphorylations of analyzed proteins were stable and peptide extracts were devoid of abundant protein degradation fragments [48]. However, it should be noted that after treatment with the Stabilizor T1, the tissues could be more fragile and therefore difficult to handle. Goodwin *et al*. [49] have reported that changes to the tissue structure have also been found to have a negative effect on the quality of the imaging MS data, although they improved the stability. Given this information, it is imperative in clinical investigations that tissue collection protocols should be standardized to reduce the likelihood of sample-processing artifacts.

8.2.2 Sample Preparation

8.2.2.1 Wash. Washing the tissue sections before matrix deposition has proven to be useful to improve spectra quality by increasing the ion yields and the number of signals observed [50]. One of the main purposes of washing tissue sections is to remove salts, lipids, and excessive amounts of hemoglobin to enhance MALDI signals. The most common washing procedure consists of a 30-s wash in ice-cold 70% ethanol

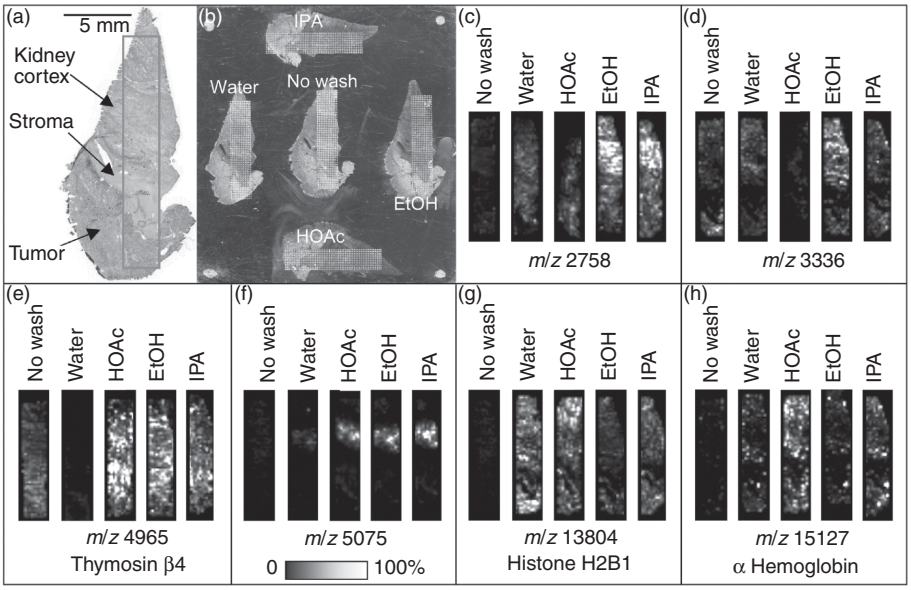

Figure 8.4 Imaging MS analysis of serial sections cut from a clear cell renal cell carcinoma resection not washed or after washing with isopropanol, ethanol, acetic acid, or water. (a) Photomicrograph of a serial H&E stained section detailing the histology of the biopsy. Areas of normal kidney cortex, stroma, and tumor are visible. The area outlined was analyzed. (b) Photomicrograph of the sections used for IMS (ion mass spectrometry) after washing and automated matrix deposition. (c–h) Ion density maps for selected protein signals from the unwashed and washed sections [50]. HOAc, acetic acid; EtOH, ethanol; IPA, isopropanol. (See color insert.)

to remove salts and cell debris, followed by a 100% ethanol wash to dehydrate and fixate the tissue. For the removal of lipids, tissue sections can be washed in organic solvents, for example, chloroform or xylene [47]. In general, the washing conditions must be optimized for specific imaging MS experiments since different tissues may require different washes.

The washing strategy also influences which biomolecules can be analyzed. Seeley *et al*. [50] systematically explored the effects of several solvent combinations for washing tissue sections. Different molecules were detected after different washes, so combining different washes can create complementary data sets describing different molecules (Fig. 8.4) [50].

It is important to be aware of the fact that there is always a potential risk of molecular diffusion during any wash procedure. Tissue sections that are fixed can be kept for several days (up to seven) in a desiccator without noticeable degradation of MALDI spectra [45]. For small-molecule analysis, such as drugs and metabolites, the wash procedures are usually omitted as they may easily delocalize the analyte of interest.

Several methods have been reported that attempt to reverse formalin fixation to "retrieve" antigens. Antigen retrieval typically involves the application of a high temperature treatment along with the use of a buffer solution, in an effort to reverse protein cross-linking and return the tissue to its native state [40]. A schematic representation is given in Fig. 8.5. First, the paraffin is removed from the FFPE sections

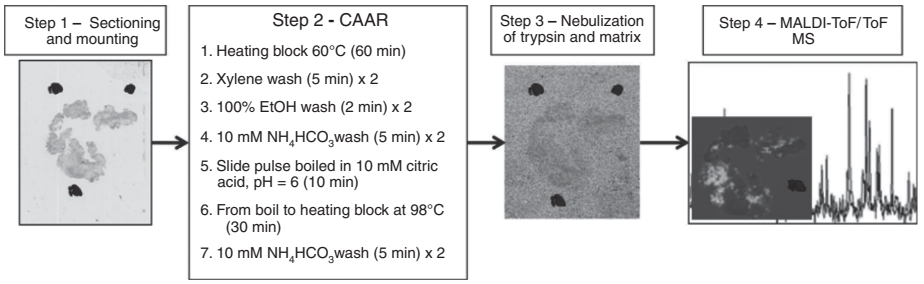

Figure 8.5 Citric acid antigen retrieval (CAAR) method applied to imaging MS of FFPE tissue. In step 1, sections cut from the FFPE block are mounted onto an ITO-coated slide. Step 2 describes the antigen retrieval process. In step 3, the proteins are cleaved into proteolytic peptides and then extracted by the deposition of the MALDI matrix solution. Step 4 shows an example of the mass spectra and images that can be obtained [53].

using xylene (100%, twice for 20 min), followed by graded ethanol washes (100%, twice for 5 min, and successive washes of 95%, 80%, and 70% ethanol for 5 min). Then the tissue can be treated either by heating the section in a tris-EDTA buffer pH 9 at 95° C for 20 min [51,52] or by using a high temperature citric acid buffer [53].

The methylene bonds are difficult to break without destroying the peptide backbone. To solve this problem, endopeptidases such as trypsin are used directly on tissue sections to break down the protein network and retrieve the digested peptides that can additionally be used for protein identification [28].

Detection of intact proteins of a molecular mass >25 kDa has been much less successful than that of peptides and small proteins. One strategy to analyze those proteins is based on proteolytic digestion of the tissue's proteins followed by MALDI imaging MS of their tryptic peptides. In principle, this "bottom-up" strategy could enable proteins of any mass to be detected. The disadvantage is that all information regarding protein isoforms is lost. For example, in an on-tissue digestion investigation, the glucose-regulated protein 78 kDa (Grp78) was identified as being associated with human pancreatic adenocarcinoma (often referred to as *pancreatic cancer*). However, in a subsequent article, Scholz *et al*. [54] reported that several Grp78 isoforms in murine pancreas displayed significant changes solely due to postmortem protein degradation (F-test $p < 0.05$). It is much more difficult to control protein degradation in human tissue samples, and unless the tryptic peptides contain the specific posttranslational modifications of a protein's isoforms, information regarding protein isoforms is omitted.

Several strategies based on tissue washes have been developed to detect proteins of higher molecular mass. For example, a 28-kDa integral crystalline lens membrane protein could be detected after extensive washing with water to deplete highly abundant soluble proteins, followed by application of a matrix solution containing a high percentage of organic solvent [55]. This procedure would be difficult to apply as a general strategy as its success is based solely on extensive on-tissue protein purification of membrane proteins (which remain anchored to the insoluble membrane during the repeated water washes).

Another strategy has used a layered matrix preparation that enabled proteins in the 25- to 50-kDa range to be detected. It was found that Triton X-100, compatible with MS up to a concentration of 1%, aided in the detection of higher m/z proteins from tissue [56]. In short, a tissue section is placed on a drop of sinapinic acid (SA,

3,5-dimethoxy-4-hydroxycinnamic acid) matrix dissolved in 90% EtOH and 0.5% Triton X-100. Once dry, a drop of SA/xylene suspension was placed on top of the tissue section, followed by a layer of SA/90% EtOH and a layer of SA/50% acetonitrile (ACN). Franck *et al*. [57] developed a sample preparation strategy using the solvents 1,1,1,3,3,3-hexafluoro-2-propanol (HFIP) and 2,2,2-trifluoroethanol (TFE) for detection of high mass proteins with MALDI MS. Unfortunately, the very low viscosity and harsh chemical abrasiveness of HFIP and TFE make it difficult to apply this procedure with the automated sample preparation stations commonly used for MALDI imaging MS.

8.2.2.2 Matrix. The correct choice of matrix is crucial for a successful MALDI imaging MS experiment. The matrix, usually an aromatic acid, is used to absorb energy from the irradiating light source (usually a UV laser). Ablation of the matrix and gas-phase chemistry leads to the generation of gas-phase pseudomolecular ions [58]. Depending on the mass range analyzed and chemical properties of the molecules of interest, the matrix and solvent conditions should be chosen accordingly [36,45, 59–61].

The matrix α-cyano-4-hydroxycinnamic acid (CHCA) is commonly used for lower molecular weight masses (peptides <3000 Da), while SA is used for higher molecular masses (peptides >3000 Da and proteins). Phospholipid analysis typically involves either 2,5-dihydroxy benzoic acid (DHB) or 2,6-dihydroxyacetophenone (DHAP), and finally, CHCA and DHB are also often used for pharmaceuticals [62,63]. Ionic matrices, composed of a binary mixture of the matrix and a base (e.g., CHCA with aniline or *N*, *N*-dimethylaniline), have been reported to provide increased sensitivity and higher resistance to vacuum sublation [47]. The matrix 9-aminoacridine (9-AA) is used for the analysis of acidic metabolites and glycerophospholipids [64,65]. A summary of different matrices is given in Table 8.1.

The goal of the matrix solution is to effectively dissolve the analyte of interest and thus extract it from the tissue. The matrix solution typically consists of an organic solvent such as ACN or methanol, water, the matrix, and trifluoroacetic acid (TFA). The solvent composition, the matrix concentration, and the TFA concentration have all been shown to affect the protein profile obtained from a tissue [32]. It is for this reason that the matrix solution needs to be optimized for each application and then carefully and reproducibly applied to the tissue in order to obtain images that accurately represent the distribution of the molecules of interest within the tissue [32].

8.2.2.3 Matrix Application. MALDI MS requires the presence of matrix crystals. Imaging MS has been used to investigate the distribution of analytes within matrix crystals and has indicated a partial segregation within and between the crystals [66].

TABLE 8.1 A Summary of Matrices used in MALDI Imaging MS Experiments

Abbreviation	Chemical Name	Application
DHB	2,5-Dihydroxybenzoic acid	Lipids, peptides, carbohydrates
CHCA	α-Cyano-4-hydroxycinnamic acid	Peptides
SA	Sinapinic acid	Proteins
DHAP	2,6-Dihydroxyacetophenone	Lipids
PA	Picolinic acid	Oligonucleotides
9-AA	9-Aminoacridine	Metabolites

To avoid such artifacts, the matrix crystals need to be significantly smaller than the pixel size of the image. For imaging MS of peptides and proteins, the most common application, the analyte molecules need to be incorporated into the growing matrix crystals for high sensitivity analyses. In general, larger crystals have extracted more analyte from the tissue, leading to higher signals, but generate lower spatial resolution images. Smaller crystals maintain high spatial fidelity, enabling higher spatial resolution images to be obtained, but contain less extracted analyte and are thus associated with lower sensitivity.

Initial imaging MS experiments used a manual TLC (thin-layer chromatography) sprayer to apply a uniform matrix layer onto the tissue, and this remains one of the first methods used by new groups entering the field because of its low cost. However, it is generally associated with low reproducibility and the use of one of the commercially available automated systems is strongly recommended. These devices are based on either microspotting or spray deposition. The microspotters sequentially deposit 100- to 200-pL droplets of matrix solution according to a predefined array, whereas the sprayers deposit sequential layers of small droplets over the sample.

The important factors to consider are how does the deposition method affect extraction of the tissues' peptides and proteins? and does the deposition method influence matrix crystallization? Sequential deposition of tens of 100- to 200-pL-sized droplets, such that each position of the array is sampled using nanoliter-sized droplets of matrix solution, has been found to be highly effective at dissolving peptides and proteins in the tissue and incorporating them into the matrix crystals. For efficient extraction, the spray devices need to apply a sufficiently "wet" layer of matrix onto the tissue, but care must be taken to avoid depositing too many droplets onto the tissue, as flooding causes lateral migration. Several instruments have been developed to apply the matrix, for example, the ImagePrep device (Bruker, Germany) and the TM Sprayer (Leap Technologies, USA). The ImagePrep device attempts to prevent flooding and control matrix deposition by using an optical sensor to monitor the sample's wetness as well as the thickness of the matrix layer. Alternatively, the TM Sprayer uses a heated spray to ensure more rapid solvent evaporation. Using these commercial spray devices or a laboratory-built system to deposit multiple layers of matrix solution (incorporating multiple steps of peptide and protein extraction, redissolution, and recrystallization) a uniform layer of peptide/protein-doped matrix crystals can be obtained. Following matrix coating, samples maybe coated with a thin layer of metal such as gold to avoid sample charging and thereby increase the detected signals [39,40].

Several solvent-free matrix dry-coating methods have been developed for small-molecule analysis. Matrix sublimation can produce an even layer of small crystals across the tissue section [67]. The deposition can be readily controlled with time, temperature, and pressure settings and is highly reproducible from one sample to the next. This technique eliminates the potential for analyte migration during solution-based matrix application and produces very small crystals that are necessary for high spatial resolution measurements. However, the dry-coating approach is not suitable for peptide or protein analysis because these compounds need to be incorporated into the matrix crystals.

For the detection of lipids on tissue sections, a 20-μm sieve has also been used to deposit finely ground matrix onto tissue. The lipid signals obtained were comparable to those from spray-coated sections, producing identical localization patterns even with this simpler and faster sample preparation [68]. This approach was found to yield highly

reproducible results, eliminating much of the variance caused by operator differences and making it an attractive alternative to solvent-based methods. A similar method uses a ball-mill device to press the matrix through a metal mesh. The mesh (20 μm) produces 1- to 12-μm crystals (DHB, CHCA matrices) in 1 min, as determined by optical microscopy, permitting fast uniform matrix coverage. Even 1- to 5-μm sized crystals could be obtained using a 3-μm mesh [69].

8.2.3 The Experiment

8.2.3.1 The Spatial Resolution. The spatial resolution of an imaging MS experiment determines the size of the spatial features that can be resolved. The resolution is dependent on the sample preparation, signal intensity per pixel, the capabilities of the instrument (laser spot on target), and the distance between raster points. The laser spot size is dependent on the ion source, the focusing optics, and the geometry of the source. The spatial resolution desired is an important factor in determining the method of matrix application.

Imaging by using an array of small discreet droplets, deposited using an automated spotting device, limits sample migration to within the diameter of the matrix droplet, typically ≈150 μm. An array of such spots, with a 200-μm pitch, would be referred to as having a spatial resolution of 200 μm.

Recently, McDonnell *et al*. [70] indicated the protein concentration range accessible for MALDI imaging MS (Table 8.2). The table shows the amount of a specific protein in each pixel as a function of spatial resolution, tissue thickness, and protein concentration. Assuming a detection limit of 1 attomol (10^{-18} mol), a 10-μm pixel is the highest spatial resolution achievable for a 1-μM peptide present in a 10-μm-thick tissue section. At smaller pixel sizes, there is simply insufficient peptide/protein available to detect it using current MALDI strategies. In practice, the achievable resolution will be less because the efficiency of protein extraction, ionization, and detection is lower than 100%. Without significant improvements in sensitivity, high spatial resolution analysis will be limited to more abundant species that ionize well, such as lipids or peptides in endocrine tissues [70]. For example Rompp *et al*. [71] have reported high mass resolution and high spatial resolution (around 5 μm) of lipids and peptides in pituitary tissue.

The spatial resolution limitations highlighted here refer to the amount of protein present in a voxel and thus would also apply to a profiling workflow utilizing laser-capture microdissection, protein extraction, trypsin digestion, and LC-MS/MS. MALDI analysis of tissues can generate mass spectra containing hundreds of distinct peptide and protein peaks from a single 150 × 150-μm pixel. Assuming an average cell size of 20 μm, this corresponds to < 60 cells. This is much smaller than the samples typically analyzed in a proteomics workflow using protein extraction and LC-MS/MS analysis and is a testament to the successful on-tissue fractionation of the ion, lipid, peptide, and protein components. Cornett *et al*. [12] have shown how the specificity and reproducibility of direct tissue profiling can be similar to those obtained using laser-capture microdissection but used far fewer cells.

8.2.3.2 Identification. In an imaging MS experiment, different proteins are distinguished and characterized by their intrinsic molecular mass; however, additional experiments are necessary to assign identities to these masses. In-source decay can be used to obtain N-terminal sequence information to identify proteins in a "top-down" strategy [72]. However, the lack of a precursor ion selection step can make

TABLE 8.2 Total Amount of a Specific Protein as a Function of Pixel Size, Tissue Thickness, and Protein Concentration[a]. Combinations highlighted in green may be considered accessible in a modern MALDI ToF mass spectrometer

	Tissue Thickness 10 µm					Tissue Thickness 2 µm	
Concentration [M]	100 µm	50 µm	20 µm	10 µm	5 µm	5 µm	2 µm
1.00E−03	100 fmol	25 fmol	4 fmol	1 fmol	250 amol	50 amol	8 amol
1.00E−04	10 fmol	2.50 fmol	400 amol	100 amol	25 amol	5 amol	0.8 amol
1.00E−05	1 fmol	250 amol	40 amol	10 amol	2.5 amol	0.5 amol	0.08 amol
1.00E−06	100 amol	25 amol	4 amol	1 amol	0.25 amol	0.05 amol	0.008 amol
1.00E−07	10 amol	2.5 amol	0.4 amol	0.1 amol	0.025 amol	0.005 amol	
1.00E−08	1 amol	0.25 amol	0.04 amol	0.01 amol	0.0025 amol		
1.00E−09	0.1 amol	0.025 amol	0.004 mol	0.001 amol			
1.00E−10	0.01 amol	0.0025 amol					
1.00E−11	0.001 amol						
1.00E−12							

[a]Ref. 70.

in-source decay more difficult to apply to the analysis of complex samples such as a tissue section. Furthermore, the low charge state (the majority of MALDI-generated ions have unit charge) and large size of proteins make ion activation methods such as collision-activated dissociation inefficient. For these reasons, protein identification is normally performed using LC-MS/MS of tissue extracts or via on-tissue digestion protocols [39]. On-tissue digestion protocols deposit a trypsin solution in the same way as used for matrix application, thus forming proteolytic peptides of each protein while maintaining their original spatial distribution. Several groups have now demonstrated that on-tissue digestion combined with MALDI imaging MS can be used to identify and localize proteins through their tryptic peptides; among others, it has been applied to lung cancer [28], breast cancer [51], prostate cancer [73], and pancreatic adenocarcinoma [74]. Recently, N-terminal peptide derivatization strategies were shown to provide improved peptide identification by directing the fragmentation to provide a complete *y*-fragment series [75]. The increased complexity of the composition of the tissues following on-tissue digestion (every protein will form many different proteolytic fragments) means that on-tissue digestion and MALDI imaging MS analyses reporting new protein biomarkers will still need to be independently verified using additional means. Cazares *et al*. [73] recently used a combination of intact peptide and protein MALDI imaging MS, on-tissue digestion, and immunohistochemical staining (IHC) to demonstrate the localization of a new candidate protein biomarker in prostate cancer tumors. To identify lipid species, preliminary peak assignments can be obtained from the LIPID MAPS database (http://lipidmaps.org) and then further confirmed by performing MS/MS analysis. Neutral losses can provide headgroup information as well as identify the fatty acid groups of the lipids [76].

8.2.3.3 Mass Analyzers. Imaging MS has benefitted from recent technological innovations in the MS field. The most commonly used mass analyzers for imaging MS are ToF (time of flight) (linear, reflectron, and orthogonal), quadrupoles, hybrid instruments such as ToF/ToF or Q-ToF (quadrupole time of flight), ion-mobility ToF, and ion trap (IT) (QIT, Orbitrap, and FT-ICR (Fourier transform ion cyclotron resonance)). An overview of the commercial instruments that are used in the MALDI imaging MS field and their performance capabilities can be found on www.maldi-msi.org.

The majority of MALDI imaging MS is performed using ToF mass analyzers because they offer the combination of parallel detection of a broad mass range, high sensitivity, and high speed. The linear geometry is commonly used to image proteins because of the need for a high mass range, while the reflectron geometry is used to resolve and identify endogenous peptides and tryptic peptides [this geometry is more limited in mass range (<6 kDa)]. An orthogonal ToF enables the performance of the mass analyzer to be independent of the ionization step, thereby maintaining optimum performance of the mass analyzer throughout the tissue section [77]. The addition of ion mobility to a mass analyzer adds an additional, partially independent, separation dimension that distinguishes between ions on the basis of their gas-phase cross section and thereby further improves the separation of drugs, metabolites, lipids, and peptides [78]. The Fourier transform techniques, FT-ICR and Orbitrap, provide very high mass resolution capabilities, which can distinguish between isobaric species and thus is very useful for imaging lipids, drugs, and metabolites [79].

The detection sensitivity of the typical microchannel plate detector used in a ToF mass analyzer decreases at higher m/z because of the lower intrinsic ion-to-electron

conversion efficiency of slower moving ions and detection saturation [80]. When a ToF MS is equipped with a high mass detection system (CovalX, Switzerland), the detection of macromolecules, up to 1.2 MDa, with nanomolar sensitivity can be achieved. Recently, we showed that this detector with the sample preparations described above allowed the detection of large ions (>50 kDa) direct from tissue with higher sensitivity [81].

Hopfgartner *et al*. [82] have reported the use of a multiple reaction monitoring (MRM) instrument for MALDI imaging of pharmaceuticals and their metabolites in whole-body sections. MRM instruments can provide higher sensitivity than other mass analyzers, as well as very high speed, but require the mass and tandem mass spectra of each analyte of interest to be known before the experiment. MALDI MRM imaging is limited to the analysis of a small number of species owing to the finite number of laser shots that can be applied to a specific region of tissue and still yields biomolecular ions; nevertheless, the high sensitivity and high speed of the technique could make it a powerful tool for validation of candidate biomarkers in clinical tissue cohorts [83].

These examples demonstrate that high quality MALDI imaging MS experiments can be performed with most modern MALDI mass spectrometers, provided the samples have been prepared well. Sample preparation and the analysis of the resulting data are frequently the limiting factors in the workflow. Newly released MALDI mass spectrometers continue to offer improvements in speed, higher mass resolution, higher spatial resolution, and additional separation dimensions; all of which combine to generate larger data sets that need to be efficiently analyzed to take full advantage of the improved data quality and quantity.

8.2.3.4 Quantitation. Tissue-specific response curves have been used to quantify the amount of drug compounds in animal tissue. A dilution series of drug standards is applied on a set of tissues and the average response curve is determined [63]. For whole-body imaging MS experiments, it has been reported that the determination of relative response factors, for each organ in the whole-body section, could provide quantitative results in agreement with whole-body autoradiography [84]. This was performed by applying a uniform coating of the drug over an adjacent section and using the MALDI-generated ion signals to determine a relative response. Robust sample preparation methods of identical MALDI imaging MS experiments are crucial for quantifying MS images [63,85].

8.2.3.5 Integrating Histology and Imaging MS. A very important aspect of imaging MS analysis of tissue is to correlate the MS images with the morphological structures shown in histological images. Since the introduction of ITO glass slides, which enabled staining and imaging MS of the same tissue section [86], it is now a more common procedure to H&E stain the tissues after imaging MS analysis. After the measurement, the matrix is removed by washing the sections in 70% methanol twice for 30 s, followed by a standard H&E staining protocol. The optical image of the stained sections can then be coregistered with the MS image. The pathologist can annotate areas of particular interest, enabling a direct comparative analysis of the biomolecular signatures obtained from the specific histology features. Such histology-defined analyses have already led to the identification of several novel biomarkers, for example, in human brain tumors [11,23,27,28,73,87].

There are stains available, such as cresyl violet, Terry's polychrome, methylene blue, nuclear fast red, and toluidine blue, that are MS compatible with a minimal risk of protein delocalization [86]. These nuclear stainings can be of great help in providing higher accuracy for the imaging MS by focusing on specific morphological regions of interest. This technique can also be used in laser-capture microdissection to allow capture and direct analysis of specific cells of interest. Cornett *et al*. [12] have used histology-directed profiling to record the biomolecular profiles of different cell types.

8.2.3.6 Data Analysis. The analysis of imaging MS data can be separated into three distinct steps, namely, data preprocessing, statistical analysis, and visualization. Figure 8.6 shows a schematic representation of the data acquisition, data processing, and correlation strategies, which can be used [88]. First, the mass spectra are processed to reduce random noise (mass spectral smoothing), remove the nonspecific background signal prevalent in MALDI-MS spectra from tissue (background subtraction), correct for inhomogeneities in the matrix coverage (total-ion-count (TIC) normalization), and finally, align every pixel's mass spectrum onto a common m/z scale (mass spectral alignment). It has been shown how each of these steps can significantly improve the qualitative and quantitative information obtained from imaging MS experiments [88].

The statistical analysis performed on imaging MS data sets is largely determined by the goal of the experiment. MALDI imaging MS generates large and highly dimensional data sets that can describe the distributions of hundreds of peptide and protein signals. A comparative analysis of the different cell types in a tumor, as defined by histology, can be used to identify biomarker peptides and proteins specific to each cell type or to find peptide and protein profiles (incorporating multiple peptides and proteins)

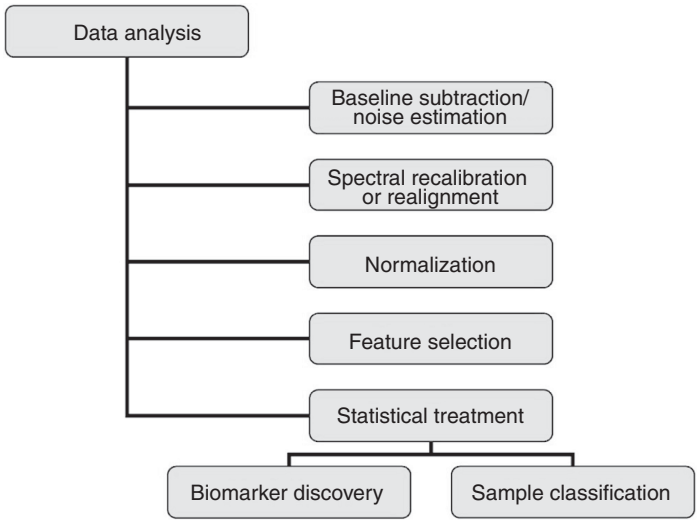

Figure 8.6 Data processing and analysis workflow. The mass spectra are processed by removing the background signal, alignment of each pixel's m/z scale, normalization to each pixel's TIC, and finally peak selection. The reduced data from peak selection can then be subject to statistical analysis in order to identify specific features that discriminate between two (or more) specified classes, biomarker discovery, or to classify tissue based on their biomolecular content [88].

that discriminate between the different cell types. Such supervised, histology-defined classification of tissues has been performed using several different tools, including linear discriminant analysis [26], genetic algorithms [23], and support vector machines [23,28]. Groseclose *et al*. [28] used MALDI imaging MS to analyze a tissue microarray containing 112 needle-core biopsies from lung tumors diagnosed as adenocarcinoma and squamous cell carcinoma. A support vector machine classifier based on 73 tryptic peptides enabled regions marked as adenocarcinoma by a pathologist to be classified with an accuracy of 97.9% (140/143 spectra) and squamous cell carcinoma with an accuracy of 98.6% (141/143 spectra).

These classification studies are based on the prior histological annotation of the tissue. One of the potential advantages of MALDI imaging MS is that it can define a tissue based on its peptide and protein signature and thereby identify regions that display a molecular signature associated with a tumor but which have not yet undergone morphological transformation. For example, MALDI imaging MS analysis (supported by LC-MS) found colorectal-carcinoma-related proteins in histologically benign polyps, from which the authors inferred that these apparently benign polyps could have malignant potential [89]; recently, Willems *et al*. [90] demonstrated that imaging MS could reveal the intratumor heterogeneity of intermediate-grade myxoid fibrosarcoma tumors (which showed the same nodal structure in multiple patient samples).

A variety of data-analysis tools have been applied to examine the innate correlations within MALDI imaging MS data sets [26]. The most common, principal component analysis (PCA), is an unsupervised multivariate technique that maximizes the variance (spread) in the data to identify the peptides or proteins that are responsible for the largest variation in the data set [91]. The result is a series of orthogonal principal components (PCs) that describe, in descending order, the maximum variance in the data set, the next maximum variance (orthogonal to PC1), and so on. PCA is adept at finding the major variances within the data sets but will only reveal the molecular distributions of interest if the peptides and proteins have sufficient signal to noise (for their distributions to be described in earlier PC's than the noise). One of the tools beginning to establish itself in MALDI imaging MS is hierarchical cluster analysis [27]. This technique groups the pixels according to a hierarchical ordering of the similarity of their spectra. The resulting dendrogram displays the hierarchy and provides a simple tool to investigate the relationships between the pixels and thus to navigate the spatial variation of the tissue's peptide and protein profiles.

An imaging MS analysis creates a mass spectrum for every pixel of the image, each of which contains a multitude of peaks that describe the mass and intensity of specific biomolecules. These rich multiplex analyses generate very large data sets, which has limited most analysis of the innate variation in the biomolecular content of the tissue to a small numbers of tissues. Recently, McDonnell *et al*. [92] developed automated feature detection and extraction algorithms for imaging MS data sets that can effectively distill each pixel's mass spectral data into the features of interest and thereby reduce the data load by $\times 100-1000$.

Finally, the visualization of 2D and 3D imaging MS data, whether the distribution of a single species or the results of a statistical analysis, is typically achieved using false color images. It is recommended that the user limits the number of channels (masses or results of data analysis) to a maximum of three. Three channels can be effectively communicated using RGB scales and clearly display overlapping regions in another color. A number of software packages are available to generate images from data

generated in an imaging MS experiment, for example, BioMap, Fleximaging, Axima2 Analyze, and Image Quest.

8.2.4 Novel Approaches—Targeted Analysis, Tissue Stretch, and Automation

Several methods have been developed that provide new variations to the imaging mass technique.

8.2.4.1 Targeted Imaging MS. This technique has been developed to enhance the specificity of the analysis. Functionalized antibodies carry a photocleavable reporter group that, can be detected by MALDI MS. The antibodies interact with an antigen of interest, and the localization of this antigen can be determined by analyzing the photocleavable probe. Two different methods have been developed: TagMass [71] and TArgeted multiplex MS IMaging (TAMSIM) [93,94]. The TagMass procedure is based on specific MALDI imaging of proteins using a probe labeled with a photocleavable linker attached to a small peptide. The small peptide acts as the reporter molecule detected in the mass spectrometer and thus is used to image the distribution of the antigen. TAMSIM uses small, intrinsically ionic molecules as the reporters, for enhanced sensitivity. Different reporter molecules can be designed, allowing multiple markers to be tagged (Fig. 8.7) [93,94].

The tissue is incubated with the functionalized antibodies, up to three different tags have been reported in a single assay, without the risk of mutual quenching that can

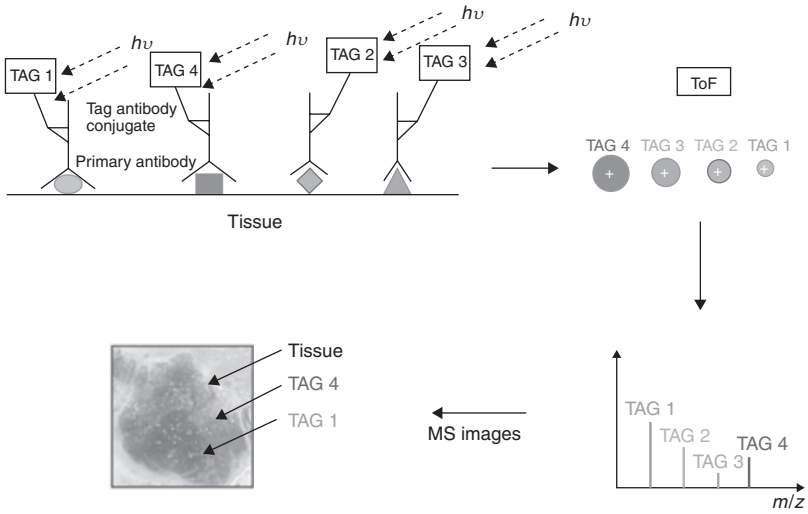

Figure 8.7 TAMSIM: mass spectrometry analysis of mass-tag conjugated antibodies. Primary antibodies are incubated with the tissue section to bind with the antigen in the tissue. Secondary antibodies that each carries a specific mass tag are specifically attached to each primary antibody. The slide containing the tissue is then introduced into the mass spectrometer, where the pulsed UV laser of the MALDI ion sources cleaves the mass tags from their antibodies and releases them into the gas phase. The m/z values of the mass tags, provided by the mass spectrometer, differentiate between the different mass tags and thus provide antigen specificity. Spatially correlated analysis enables the distribution of each antigen in the tissue [93]. (See color insert.)

occur in fluorescence imaging. After irradiation of the tissue with laser, the reporter molecules are released from the antibodies and detected in the mass analyzer. Using labeled oligonucleotide and antibody probes, Lemaire *et al*. [95] have demonstrated how TagMass can be used to record the distribution of proenkephalin mRNA and a 180-kDa membrane protein. Recently, Thierry *et al*. [93,94] used TAMSIM to localize synaptophysin, chromogranin, insulin, calcitonin, and somatostatin in pancreatic neuroendocrine cells and the cancer markers PS100 and HMB45 in human lymph node and liver invaded by metastatic melanoma. Some of these proteins are below the detection threshold in a standard imaging MS experiment. Moreover targeted imaging MS can be applied to both frozen and FFPE tissue sections.

8.2.4.2 Tissue Stretch. In this method, a tissue section is placed onto an array of glass beads embedded in a parafilm membrane [96]. By stretching the membrane, the tissue section is fragmented into small individual pieces ($\sim$40 μm in size) that can be individually prepared for MALDI-MS analysis. The physical separation between beads prevents analyte redistribution during matrix application and thus allows larger matrix droplets to be applied, thus enabling longer analyte extraction periods and increased sensitivity. This sample preparation has also been found to reduce the presence of alkali metal adducts [96]. This technology has been made more practical by the development of automated image reconstruction algorithms [97].

8.2.4.3 Automation. The low throughput of imaging MS has been one of the bottlenecks in investigating the clinical potential of using the multiplex molecular images as a novel molecular histological technique. Recently, an automated setup, consisting of a controlled environment sample storage chamber, a sample loading robot, and a MALDI-ToF/ToF MS, all controlled by a single user interface, was developed [98]. This approach in combination with the new high speed ToF/ToF instruments such as the AB Sciex ToF/ToF 5800, the ultrafleXtreme ToF/ToF from Bruker Daltonics, and the AB Sciex FlashQuant Triple Quad will provide the robustness and increased throughput for high throughput analyses.

8.3 APPLICATIONS

8.3.1 Oncology

Imaging MS can contribute significantly to cancer research as a tool to help diagnose tumors and provide indicators for the susceptibility to recurrence and progression. It can also be used as a discovery tool to detect biomarkers that are specific for early-stage tumor formation. MALDI imaging MS has already demonstrated its ability to distinguish cancerous tissue, differentiate between tumor types and tumor grades, and to locate protein biomarkers. Recently, an extensive review on imaging MS in cancer research was published by McDonnell *et al*. [70].

8.3.1.1 Brain Tumors. Meningiomas can be classified into three major grades: benign (grade I), atypical (grade II), and malignant (grade III). MALDI-MS profiling and imaging experiments of brain tumor tissues have shown how direct tissue analysis can locate gliomas as well as distinguish between the different tumor types,

grades, and subclasses [9,13,16,86,99,100]. For example, the protein thymosin β4 was found to be primarily located in the proliferating head of the tumor, whereas the protein S100A4 was found localized in the tumor core [16].

Chaurand *et al*. [101] have shown how the levels of the calcium-binding protein S100B (and independently verified using IHC) can be used to distinguish high grade and low grade glioma. MALDI profiling MS has even revealed protein profiles that are correlated with tumor histology and patient survival [17]. Statistical analysis of the MALDI-MS profiles from 108 glioma patients, or the subset corresponding to 57 patients diagnosed with grade IV malignant gliomas, could identify protein profiles associated with shorter-term or longer-term survival.

To further develop imaging MS for clinical applications and to develop a reference database for predictive classification of brain tumors, Agar *et al*. [102] set up a study to evaluate predictive classification of brain tumors using imaging MS. A preliminary classifier based on a support vector machine model was able to distinguish between meningioma image spectra from the nontumor brain and gliomas and thus to enable class imaging of surgical tissue. It was demonstrated that the development of the classifier was very sensitive to data preparation parameters such as recalibration and the peak picking algorithm. Similar conclusions have been previously reported for clinical profiling experiments [103]. The performance of a classification algorithm is sensitive to systematic but nonconstant variations in the data due to differential sample processing, mass analysis methods, or data-processing routines. Consequently, it is crucial for clinical applications that standardized protocols are followed.

Three-dimensional MALDI imaging [19,104] has also been applied to brain tumors, specifically 3D imaging coregistered with *in vivo* magnetic resonance imaging (MRI) [105,106]. The integration of MALDI imaging MS can help establish the molecular phenotypes associated with the anatomical features detected with MRI and may help to assess if these changes in molecular phenotype occur before anatomical transformation [89]. The distribution of the astrocytic phosphoprotein Pea15, a protein previously determined to be elevated in grade III gliomas [17], is shown in Fig. 8.8, volume rendered against the corresponding *in vivo* MRI data. Good agreement could be obtained between the areas highlighted by MRI and areas with high Pea15 content. Figure 8.8b shows a comparison of 2D overlays of the MALDI imaging MS data and different MRI coefficients, as well as the results of a region-of-interest (ROI) analysis comparing regions inside and outside the tumor (in the cortex). It can be seen that both MRI and MALDI imaging MS can distinguish the tumor. The enhanced T_1 (longitudinal relaxation time weighted), diminished T_2 (transverse relaxation time weighted), and diminished ADC (apparent diffusion coefficient) signals observed in the MRI scans may be explained by differences in cell density, water, and protein content.

8.3.1.2 Breast Cancer. Direct MALDI analysis of mouse mammary tumor virus/HER2 transgenic mouse has revealed protein profiles that appear to predict the antitumor action of molecular therapies [13]. When treated with the erbB receptor inhibitors OSI-774 and Herceptin, inhibition of proliferation and induction of apoptosis and tumor reduction were predicted by a $>80\%$ reduction in thymosin β4 and ubiquitin. The effects were time and dose dependent and confirmed by a MALDI imaging MS analysis, in which the spatial distributions of the proteins were inversely correlated with that of the small-molecule inhibitor.

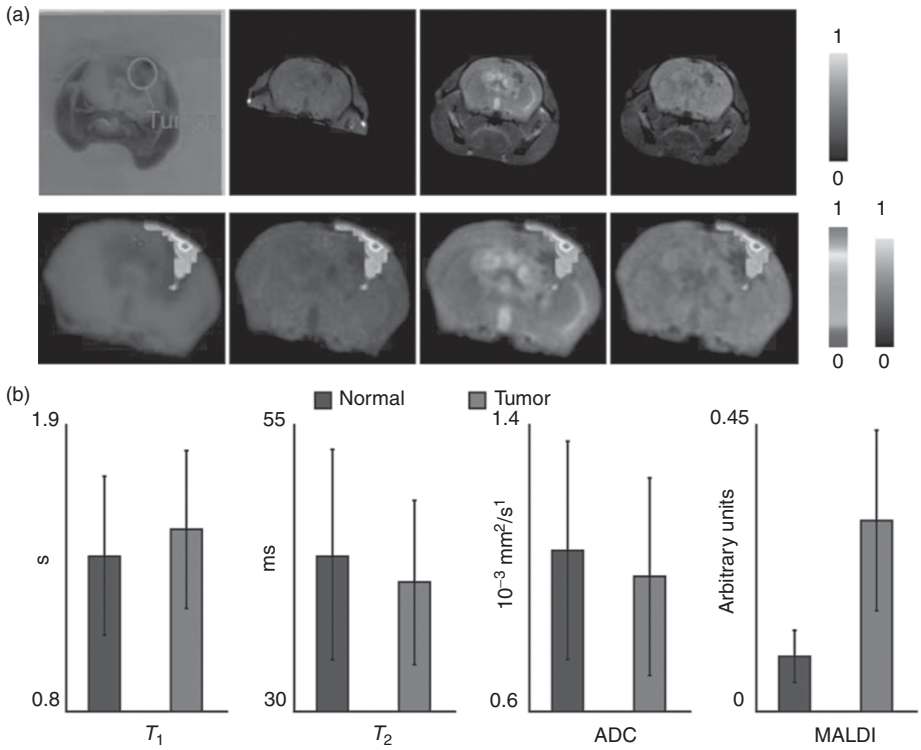

Figure 8.8 Intermodal imaging. (a) Coregistered MALDI imaging MS and magnetic resonance imaging data from a whole mouse head. (Top) Corresponding slices from coregistered blockface, T_{1w}, T_{2w}, and diffusion weighted volumes, rendered in normalized grayscale (0 is black, 1 is white). (Bottom) The same slice with the MALDI imaging MS distribution of the protein Pea 15, a biomarker for grade III glioma, overlaid. (b) Results of a ROI analysis for manually selected normal and tumor tissue [106]. (See color insert.)

Knowledge of estrogen receptor (ER), progesterone receptor (PR), and, more recently, growth factor receptor HER2/neu (ERBB2) status has been critical in the evolution of modern targeted therapy and remains essential for making informed therapeutic decisions. Recently, it was demonstrated that a multiplex assay of the mRNA of these three proteins provided significantly improved diagnostic capabilities and could provide the personal "theranostic test" to guide therapy selection [107]. Rauser *et al*. [108] have demonstrated that MALDI imaging MS may determine HER2 status directly from patient tissues. MALDI imaging MS analysis of 48 breast cancer tissue samples revealed specific peptide and protein expression changes associated with HER2 status, which could classify tissues with 83% sensitivity, 92% specificity, and an overall accuracy of 89%. The cysteine-rich intestinal protein 1 was identified as one of the proteins strongly correlated with HER2 overexpression and demonstrates how MALDI imaging MS may help develop new tissue diagnostic procedures.

MALDI MS has been used to investigate the heterogeneous nature of protein expression in breast cancer tissues [50,105]. The profiling and MALDI imaging results shown in Fig. 8.9a revealed how the different regions of a breast cancer tissue section can

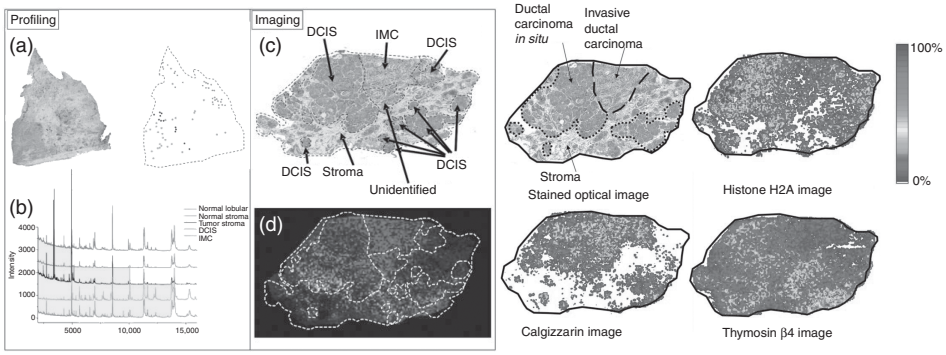

Figure 8.9 MALDI profiling versus imaging MS of human breast cancer tissue. (a) H&E stained tissue, and localized areas selected according to cell type. (b) MALDI-MS profiles obtained from cell types indicated in (a). (c) Histologically annotated H&E stained tissue section. (d) MALDI imaging MS analysis reveals distributions of specific proteins throughput the heterogeneous tissue section [105]. DCIS, ductal carcinoma *in situ*; IMC, invasive mammary cancer. (See color insert.)

generate different protein profiles. The images indicate that the individual proteins have quite heterogeneous spatial distributions but do not appear to follow the histologically annotated regions. Figure 8.9b shows the distributions of three proteins that are clearly associated with the different regions of the breast carcinoma tissue: histone H2A displays its highest abundance in the regions of the tissue histologically annotated as ductal carcinoma *in situ*, calgizzarin in invasive carcinoma, and thymosin β4 in stroma [105].

MALDI imaging MS analysis has also been performed on FFPE breast cancer tissues using in-tissue digestion protocols [51,109] or targeted imaging of a known candidate biomarker protein [110]. Instead of endeavoring to find new biomarker profiles, Seuma *et al*. [110] used Au/Ag-tagged antibodies and the quantitative elemental imaging technique, laser ablation inductively coupled plasma MS, to quantitatively image known candidate biomarkers. The technique displayed good reproducibility and quantification, with limits of detection of ≈50 fmol for both Au- and Ag-tagged antibodies. The advantage of such targeted approaches is that they can exploit the findings of the large number of serum/plasma-profiling studies that have been undertaken in recent years.

A recent systematic review on the reproducibility of MS-based serum profiling for diagnosis of breast cancer revealed that despite substantial differences in experimental design, experimental conditions, data analysis, and even analytical reproducibility, a common set of discriminating and reproducible peaks could be found, indicating the presence of breast cancer [111]. The targeted imaging of these corroborated proteins in tissue microarrays could be performed using tagged antibody strategies.

8.3.1.3 Lung Cancer. Direct tissue analysis using MALDI profiling MS has been shown to be effective for accurately classifying and predicting histological groups as well as survival in resected non-small-cell lung cancer [112]. From a data set consisting of more than 1600 distinct protein peaks, differentially expressed peaks were found that could classify lung cancer histologies, distinguish primary tumors from metastases to the lung from other sites, and classify nodal involvement. A subset of the proteins, consisting of just 15 distinct protein peaks, was found that could distinguish between

patients with resected non-small-cell lung cancer and had poor prognosis (median survival 6 months, $n = 25$) and those who had good prognosis (median survival 33 months, $n = 41$, $p < 0.0001$). The above profiling study was performed by comparing the protein signatures from 1-mm regions of tissues from 79 lung tumors and 14 normal lung tissues; consequently, each profile effectively averages the signals from the highly heterogeneous tissue in each sample area (tumor regions chosen for analysis contained a tumor cellularity >70% [112]). The same group recently used MALDI imaging MS to analyze a small lung cancer tissue microarray containing 112 needle-core biopsies. An H&E stained section of the tissue microarray was analyzed by a pathologist using light microscopy and the cancer, noncancer, and normal regions were demarcated in each needle biopsy. This annotated tissue section was then aligned with an adjacent tissue section, which was then used for in-tissue digestion MALDI imaging MS. A subset of the needle biopsies was then used as a training set, in which the origin of each mass spectrum was annotated with the histologist's diagnosis (Fig. 8.10a). Even though the data sets included tryptic peptides that were found to be located in just a subset of each specific class [28], a support vector machine based classifier using 73 tryptic peptide peaks could classify the regions in the test samples (thus not included in the training set) marked as adenocarcinoma by a pathologist, with an accuracy of 97.9% (140/143 spectra), and squamous cell carcinoma, with an accuracy of 98.6% (141/143 spectra) (Fig. 8.10b).

8.3.1.4 Ovarian Cancer. Fournier and coworkers have reported an in-depth investigation for ovarian cancer candidate protein biomarkers using MALDI profiling of tissue extracts and MALDI imaging MS, which showed that the Reg-alpha fragment of the 11 S proteasome activator complex is a new candidate protein biomarker. The candidate biomarker was identified by LC fractionation of the proteins from tissue extracts and determination of the appropriate fraction using MALDI profiling, followed by tryptic digestion and LC-MS/MS of the proteins in the fraction of interest. The results of the MALDI imaging MS investigation were then compared with IHC analysis using the anti-Reg-alpha C-terminal antibody and targeted MALDI imaging by using a primary antibody directed against the C-terminal part of human Reg-alpha and a secondary antibody modified with a photocleavable linker and a reporter peptide for MALDI-MS detection. Further analysis of the MALDI imaging data sets has demonstrated that hierarchical cluster analysis is highly effective in distinguishing the different regions of the tissue [113]. Liu *et al*. [114] used imaging MS to investigate the elevation of sulfatides in ovarian cancer in combination with transcriptomic and lipidomic approaches. In Fig. 8.11, pseudocolor ion images of sulfatides in ovarian carcinoma tissue are shown; sulfatides were only detected in the ovarian epithelial carcinoma and not in normal ovarian tissue (data not shown) [114]. Previous studies have shown that sulfatides are elevated in many types of cancer, including ovarian cancers, on the basis of colorimetric assay, which might have cross-reacted with other lipids (such as cardiolipin, phosphatidylserine, and phosphatidylinositol (PI)) [115]. Microarray mRNA data using a sphingolipid pathway map indicated that epithelial ovarian cancer cells might have elevated sulfatides, which was confirmed by LC ESI-MS/MS.

8.3.1.5 Prostate Cancer. Schwamborn *et al*. [23] have analyzed prostate cancer tissues using MALDI imaging MS to search for new and reliable candidate protein biomarkers. After the MALDI imaging MS experiment, the remaining matrix was

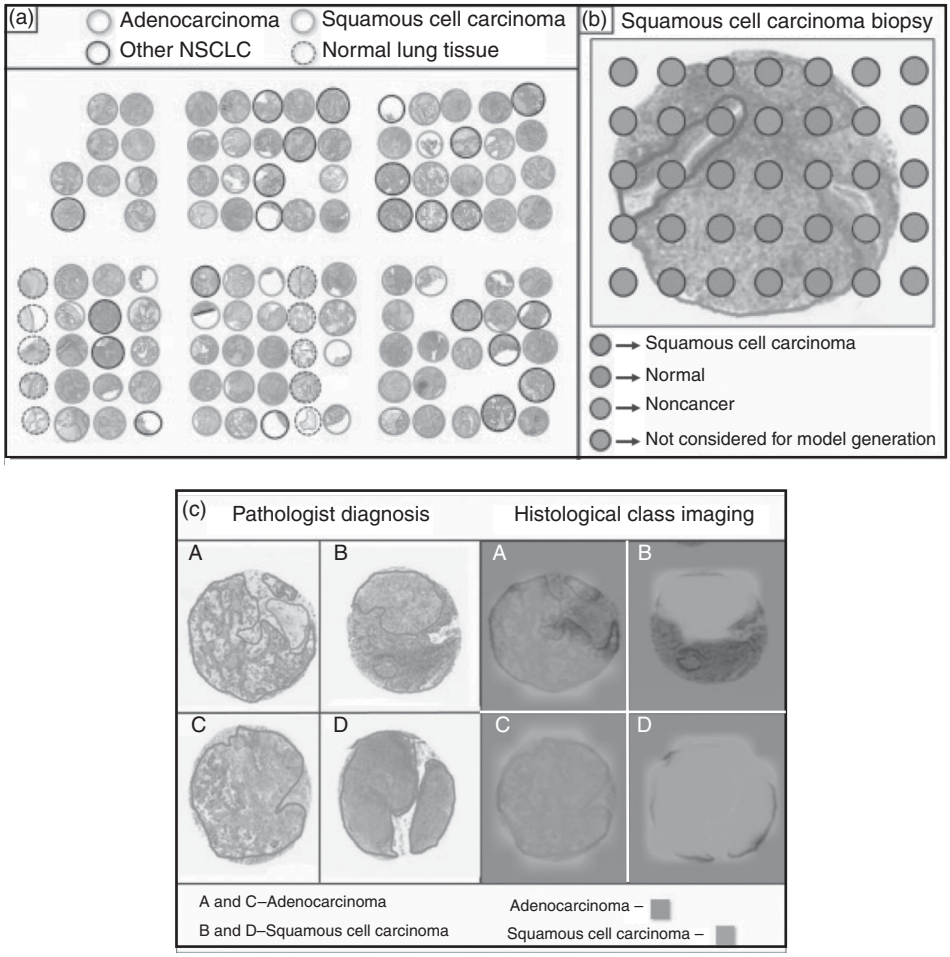

Figure 8.10 Classification of a lung cancer tissue microarray using MALDI imaging MS. (a) Optical image of an H&E stained section of the microarray and pathological diagnosis. (b) For training the diagnostic classifier, each spectrum is grouped based on the histological region from which it was acquired. (c) MALDI-imaging-MS-based classification of four biopsies compared to the diagnosis based on histology [28]. NSCLC, non-small-cell lung cancer. (See color insert.)

removed by incubating the slides twice in methanol (100%, at room temperature for 5 min) and once in acetone (100%, at room temperature for 5 min). The tissues were then H&E stained and a histological analysis performed. A support vector machine model was then built using histologically defined regions of interest (normal and cancerous areas). A false color image was created indicating those areas determined to be cancerous and compared with the results of a pathohistological analysis of the H&E stained section [23]. It was found that both regions could be distinguished with an overall cross-validation of 88% and a sensitivity and specificity of 85.21% and 90.74%, respectively, using 22 peptide and protein peaks [23]. The same data set, analyzed using just five peaks and a genetic algorithm, provided an overall cross-validation, sensitivity, and specificity of 77%, 70%, and 84%, respectively [23].

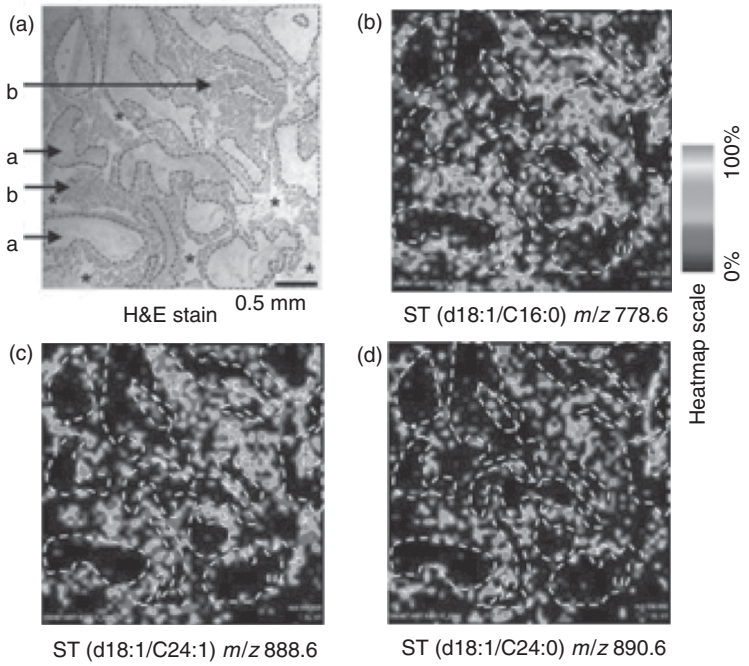

Figure 8.11 Visualization of the localization of sulfatides in ovarian carcinoma using MALDI imaging MS. (a) H&E stained thin section of an ovarian carcinoma and normal tissue. Distinctive morphological features have been outlined and superimposed on the (b–d) mass spectrometry images to aid in comparison. (b–d) Pseudocolor ion images of the ions at m/z (b) 778.6, (c) 888.6, and (d) 890.6 [114]. (See color insert.)

Cazares *et al*. recently reported a larger-scale MALDI imaging MS investigation of prostate cancer that led to the detection of a candidate biomarker. A discovery set of 11 cancer-containing tissues and 10 benign tissues was examined and a single peptide ion at m/z4355 was found that could discriminate prostate cancer from normal tissue. This finding was then verified on a separate validation set of 54 tissue sections (23 tumor and 31 benign sections). This peptide was then identified as a fragment of mitogen-activated protein kinase/extracellular signal-regulated kinase kinase 2 (MEKK2) by tandem MS analysis of tissue lysates. On-tissue digestion MALDI imaging MS detected multiple tryptic peptides of the candidate biomarker, which were colocalized in prostate cancer tumors but not in benign or normal tissue, and immunohistochemical staining of MEKK2 showed increased expression in the tumor. This clinical study highlights the potential of MALDI imaging MS to significantly contribute to patient diagnosis and to identify new candidate biomarkers: in this case, MALDI imaging MS provided the first demonstration of MEKK2 overexpression in prostate tumors and its potential correlation with cancer stage/grade [73,116].

Chaurand *et al*. [10] compared normal mouse prostates with prostate tumors derived from genetically engineered mice (LPB-Tag mouse model for prostate cancer) by MALDI profiling and imaging MS to identify proteins common to normal prostatic morphogenesis and tumorigenesis. They showed that some secreted proteins were absent in tumors, indicating that expression of these differentiated proteins is decreased

or lost during tumor cell proliferation. Cyclophilin A (CypA), a protein found in other cancers, was detected with differential αN-terminal acetylation. Immunohistochemistry and Western blot analysis demonstrated the presence of CypA both in mouse prostate tumors and in human benign prostatic hyperplasia and prostate adenocarcinoma tissue sections, although the posttranslational modifications could not be discriminated by those techniques (in contrast to the MALDI imaging MS).

8.3.1.6 Tumors of the Gastrointestinal Tract. Following the prostate cancer analysis and the lung cancer tissue microarray analysis shown in Fig. 8.10, Dijidja *et al*. [117] recently demonstrated that MALDI imaging MS could be used to classify a pancreatic cancer tissue microarray and identified a number of proteins that appear to discriminate between different tumor classes. Figure 8.12 shows the distribution of some of the observed peptide signals within the tissue microarray sections. These peptides were identified as actin, periostin, hemoglobin α-chain, and histone 2A. Figure 8.13 displays the distribution of ion signals at m/z944, 1032, and 1477 identified as histone 2A, histone H3, and type I collagen, respectively, which were found mainly in the tumor region. Figure 8.13d–f shows the H&E staining images of the section, which correspond with the MS images. All these analyses are based on tissue sections previously annotated by a trained pathologist. Although it is good practice to first test a new imaging method against established pathological analysis, such an

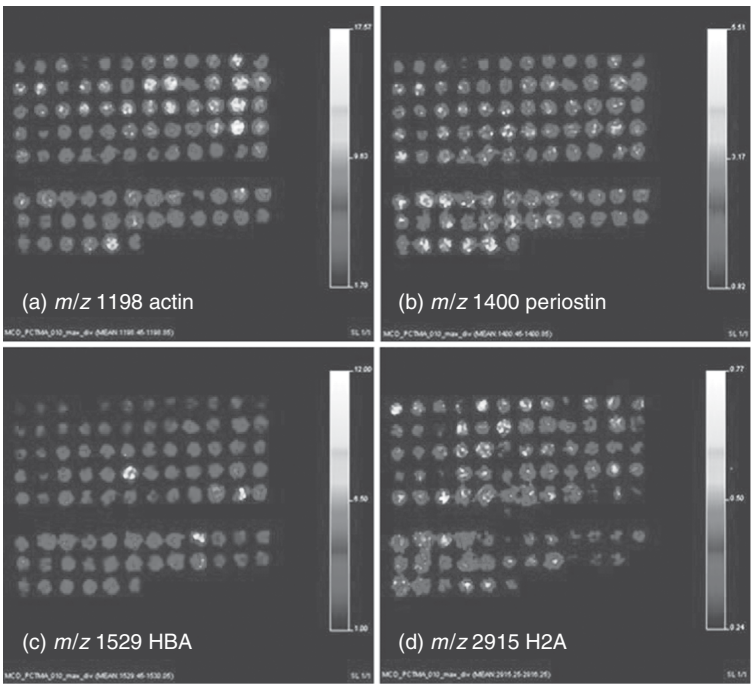

Figure 8.12 MALDI imaging MS images of the localization of proteolytic peptides within a tissue microarray. The distributions of proteolytic peptides from (a) actin, (b) periostin, (c) hemoglobin α-chain, and (d) histone H2A are displayed [117]. (See color insert.)

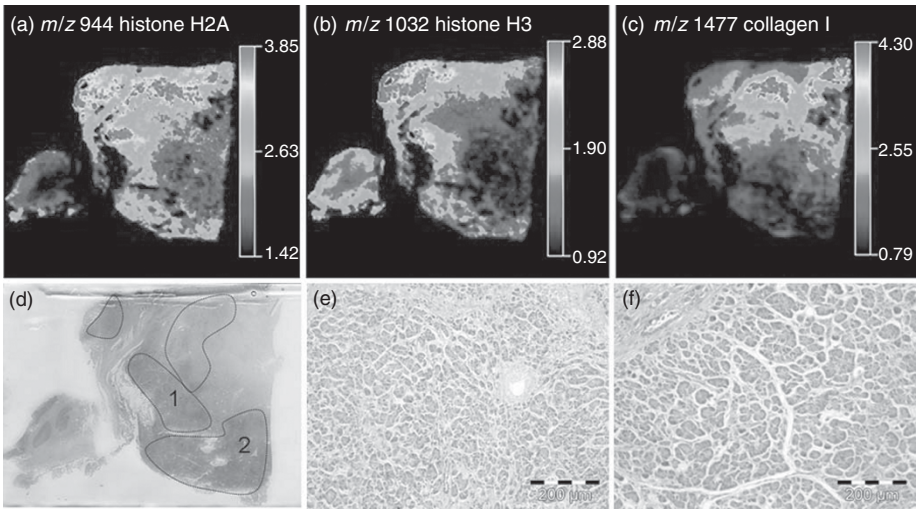

Figure 8.13 MALDI imaging MS images of the distribution of (a) histone H2A, (b) histone H3, and (c) type I collagen tryptic peptides. Images were normalized against the matrix adduct at m/z877. (d) Optical image of the H&E stained FFPE human pancreatic cancer with the localization of tumor regions. (e,f) The $\times 10$ magnification images acquired from tumor regions 1 and 2, showing tumor cells [117]. (See color insert.)

analysis will not highlight molecular differences that occur before the emergence of pathological entities.

A recent study combining MALDI imaging MS and LC-MS identified colorectal-carcinoma-related proteins in *histologically benign* polyps [89]. Examination of multiple benign polyps with MALDI imaging MS revealed colorectal-carcinoma-related proteins in the transition zone between the polyp and normal peripheral tissue, the area of greatest neovascularity and growth. This raised the concern that although a pathologist reporting no tumor in the normal tissue is correct, histology alone could underestimate the extent of preneoplastic changes (already reflected in different peptide/protein expression profiles detected by MALDI imaging MS) and progression of the lesion toward malignancy [89].

The ability to detect changes in disease-associated protein expression before their histological transformation is one of the main advantages of the nontargeted nature of the technique and arguably crucial to identify potential early-stage biomarkers. A new diagnostic method for separating benign from malignant colon polyps, based on histopathology in combination with MALDI imaging MS, may provide physicians with a more accurate diagnosis. The MALDI imaging MS measurements could also include candidate biomarkers spanning multiple molecular classes; for example, Shimma *et al*. [118] have reported that the lipids from a human colon cancer liver metastasis tissue sample clearly differentiate the cancerous regions of the tissue from the normal regions.

Gradual changes in expression levels of candidate biomarker proteins, changes in the relative levels of different proteins [15], and candidate biomarker proteins that are represented by weaker peaks in the mass spectrum require advanced data-analysis

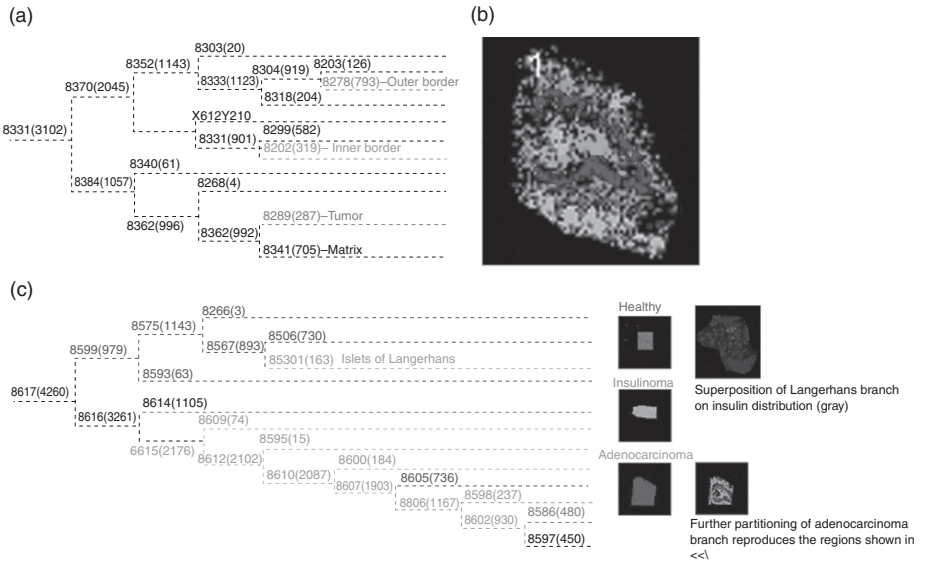

Figure 8.14 MALDI imaging MS analysis of pancreatic adenocarcinoma, insulinoma, and healthy tissue. Hierarchical cluster analysis of (a) the pancreatic adenocarcinoma data set reveals (b) the substructure in the tissue. (c) Hierarchical cluster analysis of the combined data sets distinguishes the adenocarcinoma, insulinoma, and healthy tissues as well as the substructure in the subsequent branches [70]. (See color insert.)

tools to identify or confirm the different molecular signatures associated with the different regions of the tissue. This is especially true if the goal of an experiment is to identify different regions of tissue, based on their molecular content, independent of histological analysis (e.g., to identify molecular changes that occur before histological transformation).

The hierarchical cluster analysis of pancreatic ductal adenocarcinoma shown in Fig. 8.14 clearly reveals the spatiochemical substructure of the tissue, including an area bordering the tumor core that was verified in the original MALDI imaging MS data [70]. Furthermore, it was shown that the same analysis, independent of prior histological annotation, could differentiate between healthy pancreas, ductal adenocarcinoma, and insulinoma tissue *and* indicate the different regions of each tissue.

Deininger *et al*. [27] have used hierarchical cluster analysis to highlight the different features in nonneoplastic stomach mucosa and gastric cancer tissues. After demonstrating that each histological region could be distinguished solely on the basis of their different peptide and protein profiles (thereby demonstrating the technique's capability to reproduce histological features), it was postulated that MALDI imaging MS may be able to detect phenotypic differences invisible to classical histological techniques (Section 8.3.1.7). This study was performed on a small number of surgical gastric cancer samples. Kim *et al*. [119] performed a prospective clinical study to evaluate the feasibility of using MALDI imaging MS on frozen endoscopic biopsy samples for gastric cancer from 63 gastric cancer patients and 43 healthy volunteers. Half of the samples were used to develop a classification model and were validated using the other half. It was found that both regions could be distinguished with high predictive values

(positive and negative predictive values for cancer, 96.8% and 91.3%, respectively; sensitivity 93.8%; and specificity, 95.5%) using 73 peptide and protein peaks. Signals that were overexpressed in tumors were identified as α-defensin, α-defensin/2, calgranulin A, and calgranulin/B. Furthermore, they could distinguish early stage from more advanced-stage tumors.

8.3.1.7 Intratumor Heterogeneity. One of the foremost concerns in clinical oncology and pathology is ensuring complete tumor removal [120]. Local recurrence of cancer occurs quite often, despite microscopically confirmed negative surgical resection margins, and is likely related to the presence of abnormal, fully neoplastic or preneoplastic cells adjacent to the tumor that cannot be recognized by conventional light microscopy [121]. Tumor margins can be studied by antibody-based approaches or by nuclear staining procedures, which are limited to visualization of cellular morphology [122]. Identification of proteins that define the molecular microenvironment of the neoplastic process may become an important part of the evaluation of cancer tissue, potentially helping guide surgical resection procedures. MALDI imaging MS can significantly improve the assessment of microenvironment at the molecular level and thereby not only facilitate a better understanding of tumor invasion but also provide potential markers to aid in histological assessments that help ensure complete tumor removal. Caldwell and coworkers [121,123] used this technique to reveal that changes in protein content associated with a fibrous histiocytoma can extend far into adjacent histologically normal tissue. Kang *et al*. [124] reported how MALDI imaging MS could be used to identify proteins upregulated in tumor interface zones, the region between tumors and normal tissues where epithelial–mesenchymal transition occurs. It was proposed that these proteins maybe more effective prognostic biomarkers (than proteins that are upregulated within the tumor core). Plastin 2 and peroxiredoxin 1 were identified, and independent validation of their upregulation in the interface zones of ovarian cancer was performed using fluorescence microscopy.

More recently, Oppenheimer *et al*. [29] performed an in-depth investigation of tumor interface zones of renal cell carcinoma (RCC) and revealed that normal tissue adjacent to the tumor expresses many of the molecular characteristics of the tumor. They studied the correlation of the molecular changes in the margin-normal tissue with tumor aggressiveness. Mass spectra were acquired from the tissue containing tumor and the attached normal tissue, which allowed the mapping of proteins in tumor and adjacent normal tissue. The optical image of an H&E stained section was used to define the tumor border (Fig. 8.15a). A total of 40 significant features (m/z values) were plotted for 25 patients. Most samples expressed protein patterns exemplified by line "D" in Fig. 8.15b, where features are underexpressed in the tumor and the margin as compared to the nontumor tissue. The characteristics monitored were the point at which the maximum rate of change occurred and the point at which the feature amplitude began to plateau. There was not a clear correlation between the pathological diagnosis and the distance of compromised tissue beyond the histological tumor border. For the m/z features noted, expression patterns in most samples followed the aforementioned pattern illustrated in Fig. 8.15b. There was a small group of samples in which margin trends could not be assessed [29].

The imaging MS study of gastric cancer referred to above also provided the first indication that imaging MS may help reveal heterogeneity within tumors. Hierarchical

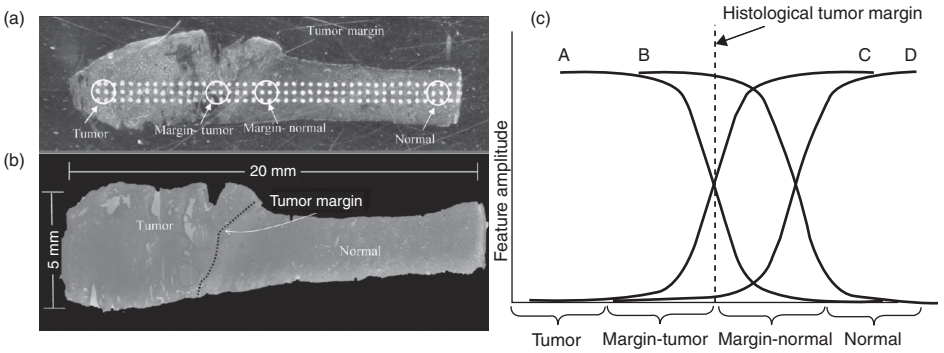

Figure 8.15 MALDI imaging MS analysis of tumor margins. (a) Optical image of tumor and adjacent normal tissue on a MALDI plate with regions of interest marked. (b) Optical image of a corresponding H&E stained section marked by a pathologist. (c) The observed patterns of the molecular features traversing the histological tumor margin. Lines A and C represent features that begin changing at the histological margin, while lines B and D represent features that change after the histological margin [29]. (See color insert.)

cluster analysis of an imaging data set revealed detailed clustering within the tumor that did not correspond to histologically distinct regions. The same data-analysis tool was recently used by Willems *et al*. [90] to demonstrate that intermediate-grade myxofibrosarcoma, a soft tissue tumor, possessed distinct areas with high-grade-like and low-grade-like character. To test if the regions could be further subdivided, on the basis of their biochemical signatures, and if the same intratumor heterogeneity is present in multiple tissues, six different localized regions of interest were selected in a single tissue sample and a support vector machine classification model was created. Application of this model to multiple intermediate-grade myxofibrosarcoma patient samples revealed that many intermediate-grade tissues exhibited significant biochemical intratumor heterogeneity. Furthermore, the results indicate that the areas previously highlighted as low-grade-like and high-grade-like consist of multiple nodules with different protein signatures. Low grade myxofibrosarcoma is microscopically characterized by a multinodular growth pattern [125]. The biomolecular heterogeneity might be due to metabolic and epigenetic differences in the tumor, though, strong evidence indicates that intratumor heterogeneity also arises from genetically distinct clones within the tumor [126,127]. Myxofibrosarcoma is characterized by nonspecific cytogenetic aberrations that increase with grade. It is thought that the tumors progress through multiple nodules, one of which becomes more dominant and progresses toward high grade myxofibrosarcoma (as has been shown in other neoplasms) [128–130]. Most human malignancies originate from a single cell but display intratumor heterogeneity by the time of diagnosis.

8.3.2 Degeneration—Neurological, Muscular, and Ocular

Molecular images of different neuropeptides have been reported, some of which were validated using immunohistochemistry [131]. Besides molecular images of peptides and proteins, different classes of lipids have also been imaged [132–138].

Wisztoski *et al*. [60] have reviewed the application of imaging MS in nervous tissues of both vertebrates and invertebrates with a focus on recent studies of neurodegenerative diseases. Langstrom *et al*. [139] have reviewed *in vitro* imaging techniques as a complement to *in vivo* positron-emission tomography (PET) and single photon emission computed tomography (SPECT) imaging in neurodegenerative diseases.

In rat brain frozen tissue sections treated with 6-hydroxydopamine, a neurotoxin commonly used to lesion dopaminergic pathways and generate experimental models for Parkinson disease, it was shown that transelongation factor 1, hexokinase, and neurofilament-M were downregulated as previously shown [140], whereas peroxidoredoxin 6, F1 ATPase, and α-enolase were upregulated [20,40]. Stauber *et al*. [40] identified three new putative biomarkers for Parkinson disease using FFPE 6-hydroxydopamine-treated rat brain tissues. Protein identification was obtained using MALDI MS direct profiling with nanoLC-nanoESI-IT MS. They confirmed that hexokinase and neurofilament-M proteins were downregulated, whereas the collapsing proteins response mediator 1 and 2, peroxidoredoxin 6, F1 ATPase, ubiquitin, and α-enolase were upregulated.

AD is a progressive neurodegenerative disorder characterized by the gradual onset of dementia. The pathological hallmarks of the disease are amyloid β plaques, neurofibrillary tangles, synaptic loss, and reactive gliosis. The localization, characterization, and quantification of amyloid β peptides have been studied in APP23 mouse brains [21,141]. Amyloid β peptides 1–40 and 1–42 were the most abundant amyloid peptides in those brain areas, which were identified by MS/MS analysis.

Scrapper, a protein which is localized at the synapses in neurons, is an ubiquitin E3 ligase that is involved in the decomposition of Rab3-interacting molecule 1, an important regulator of synaptic plasticity, and thus regulates synaptic transmission. The *Scrapper* knockout mouse brain showed two types of neurodegenerative pathologies, spongiform neurodegeneration and shrinkage of neuronal cells. In a comparison of a WT and SCR-KO mouse brains, both imaging MS and 2DE analysis detected altered molecules. There were several differences in information obtained from each procedure [142]; however, the additional value of imaging MS was that it showed the localization of several altered molecular species in the SCR-KO mouse brain spanning several molecular classes, including lipids, peptides, and small molecular weight proteins (<10 kDa), which are difficult to detect with 2DE analysis.

The *mdx* mouse is a model of Duchenne muscular dystrophy (DMD). Duchenne is a neuromuscular inherited, autosomal recessive disease. In DMD patients and *mdx* mice, modifications of the lipid composition of dystrophin-deficient muscle analyzed by radiolabeling, gas chromatography, or thin-layer chromatography [143] as well as oxidative damage [144] have been demonstrated. The most important difficulty remains the fact that in muscle biopsies, the muscle fibers are mixed with adipose and conjunctive tissues, which can be difficult to separate. The degeneration/regeneration process in muscles of *mdx* mouse was studied using MALDI-ToF profiling and cluster ToF secondary ion mass spectrometry (SIMS) imaging. Three regions in the *mdx* mouse legs could be distinguished: a severely damaged region, a second degenerating region (oxidative stress and deregulation of the PI cycle), and a third stable region [145,146]. ToF-SIMS imaging has the major advantage, over alternative methods, of allowing direct and simultaneous collection of mass spectra and ion images.

The determination of molecular composition and individual compound localization on a tissue section, at micrometer scale and without the need of any prior sample

treatment, makes the analysis easier, more straightforward, and the closest possible to physiological conditions.

Mass spectra revealed differences in the distribution of fatty acids, phospholipids, diglycerides (DGs), and triglycerides (TGs). Vitamin E and PIs were found to concentrate within the cells, whereas intact phosphocholines accumulated over the most damaged areas of the dystrophic muscles, together with cholesterol and sphingomyelin species. Fatty acyl chain composition varied depending on the region, allowing estimation of the local damage extent [147]. Recently, Benabdellah *et al*. showed inversion of the PC34:2/PC34:1 intensity ratio between destructed areas (from dystrophic muscle) and control areas (healthy muscle and structured areas from dystrophic muscle), which was interpreted as evidence of restoration of membrane lipid composition after treatment of *mdx* mice with molsidomine [64,65].

MALDI tissue profiling and imaging of proteins in ocular lenses have been developed to investigate the distribution of lens proteins [55,148–151]. Because of the lack of protein turnover, lens proteins undergo various age-related posttranslational modifications that include truncation, deamidation, glycation, and phosphorylation. The modifications accumulate over the lifetime of mammalian species and possibly contribute to lens opacification and cataractogenesis by inducing aggregation of lens proteins. While immunolabeling can be used to investigate several protein distribution patterns, its ability to simultaneously detect more than four specific antibody probes is limited principally due to the small number of discrete recording channels available. Furthermore standard immunohistochemical approaches can be challenged by the lack of specific antibodies to phosphorylated forms, the inability to detect specific truncation products, and the large number of individual experiments required to obtain this information. Molecular images showed the spatial distribution of the integral lens protein aquaporin, and its truncated products, namely, MP20, opsin, and α-crystallin, and their modified forms in one single experiment [55,148–151]. αA-crystallin was extensively degraded in the lens core; αB-crystalline degradation was limited and phosphorylation was most abundant in the middle cortex [55,148–150]. The results were validated by identification of the proteins and the modification by additional reverse-phase liquid chromatography of soluble extracts from specific tissue regions followed by tandem MS [150]. In addition, the regional distribution of lipids in porcine lens were mapped. The intraocular lens contains high levels of both cholesterol and sphingolipids, which are believed to be functionally important for normal lens physiology. Seven lens sphingomyelins and two ceramide-1-phosphates were imaged and further assigned by imaging FT-ICR MS. Glycosylated sphingolipids or sphingolipid breakdown products were not detected. Surprisingly, neither the cholesterol ion nor its dehydrated fragment ion could be detected by imaging MS, although the cholesterol molecules could be detected by SIMS and desorption electrospray ionization (DESI). This is probably due to the strong integration of cholesterol molecules in the lens [152].

8.3.3 Drugs, Tracers, and Metabolites

8.3.3.1 Drugs and Tracers. In 2003, Reyzer *et al*. [153] demonstrated that imaging MS could be used to trace the distribution of pharmaceuticals in various organs. It has rapidly developed into highly effective technique for imaging the distribution of small organic molecules, both exogenous drugs and endogenous metabolic intermediates

[154]. The advantage of this technique for metabolite imaging is that it does not require any labels or specific probes; it is a nontargeted method, and thereby many types of molecules can be analyzed simultaneously. Moreover, the parent drug and its metabolites can be distinguished [155,156], which is not possible with autoradiography or fluorescence imaging. Rohner *et al*. [157] reviewed MALDI imaging MS and described imaging work being carried out at Novartis. From the same group, there was also a report describing some of the practical aspects of obtaining imaging MS data for drug and metabolite distributions [85].

The mass range containing most drugs and metabolites can be densely populated with many ions of similar mass. Consequently, many experiments have used MS/MS to increase specificity. The increased resolving power of ion-mobility MS or FT-ICR MS enables drugs and metabolites to be distinguished using MS [132,136,155,156, 158–160]. MALDI imaging MS has attracted great interest from drug development companies. In recent years, numerous studies have been reported, where imaging MS has been used to monitor the distribution of an administered drug and its metabolites, for example, antitumor drugs (vinblastine, imatinib, banoxantrone, oxaliplatin, and diazepam) [155,156, 160–162], antipsychotics (olanzapine and clozapine) [48,119,121], antianxiety drugs and hypnotics (temazepam), treatment of chronic obstructive pulmonary disease (tiotropium) [63,163], HIV protease inhibitors [164], and an antifungal drug (ketoconazole)[62].

As described earlier, it is very important to avoid delocalization of the analyte and care must be taken when using MS to ensure there are no interfering peaks from the matrix or from endogenous compounds present in the tissue. Sample preparation procedures including the choice of matrix extraction solvents and detection method may need to be developed because of the range of structures, solubility, and physicochemical properties of drug compounds [165]. Several recent papers describe sample preparation protocols for drug imaging in which elimination of matrix-derived ions are developed such as the use of nanoparticle-based ionization [136,166], matrix-enhanced surface-assisted desorption/ionization [167], desorption/ionization on silicon [168], and nanostructure-initiator MS [169].

Imaging MS for low molecular weight compounds has been analyzed on ToF, IT, Q-ToF, IT-ToF, FT-ICR, and QqQLIT (a triple quadrupole in which the final quadrupole is a quadrupolar linear ion trap) mass analyzers [155,156]. Recent developments using MRM showed that images of a complete rat section could be accomplished with a 1000 Hz laser frequency and a rastering speed of about 18 mm/s, so a whole image of a drug compound distribution could be measured within 15 min [82].

Stoeckli *et al*. [85] and Hiesh *et al*. [84] showed that imaging MS provided detailed drug distribution images that are comparable to traditional whole-body autoradiography using radiolabeled compounds. Both methods showed high levels of a compound in several organs, while low levels in the blood were also detected. Autoradiography requires laborious and expensive synthesis and labeling of a tag with the risk of altering the pharmacological properties of the drug. Unlike autoradiography, imaging MS can distinguish the medicinally intact drugs from their metabolites. Khatib-Shahidi *et al*. [156] showed that in complete rat sections, the intact drug reached the target organ (the brain), whereas its metabolites were localized in the bladder (Fig. 8.16a).

Furthermore, the time course of the metabolism of parent drugs into demethylated and hydroxymethylated metabolites was visualized over the whole-body section (Fig. 8.16b). In this study, notable decreases of olanzapine were observed everywhere

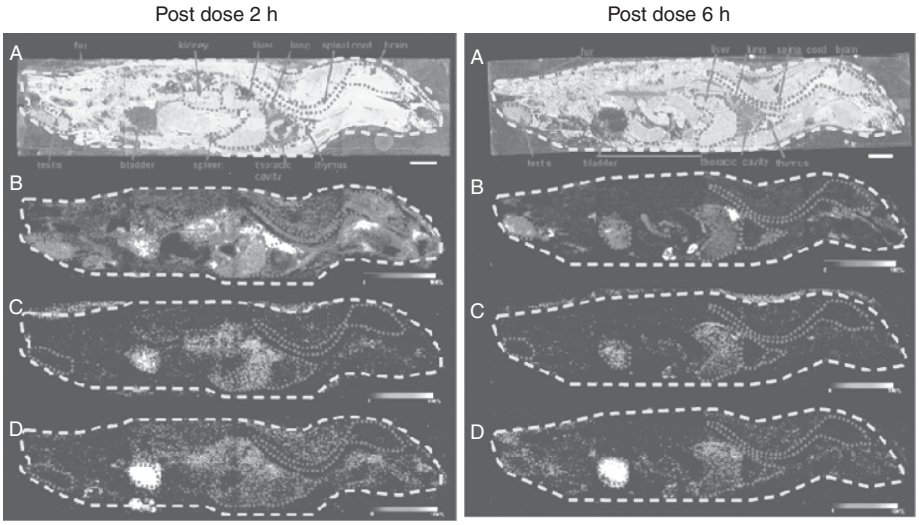

Figure 8.16 MALDI imaging MS of the drug olanzapine and its metabolites in a whole rat sagittal tissue section (a) 2 h post dose and (b) 6 h post dose. (A) Optical images of tissue sections, in which the organs have been outlined with a dark gray dotted line. (B) MS/MS images of olanzapine (m/z 256). (C) MS/MS ion image of *N*-desmethyl metabolite (m/z 256). (D) MS/MS ion image of 2-hydroxymethyl metabolite (m/z 272). Scale bar = 1 cm [156]. (See color insert.)

in the body except the testis and bladder, while the metabolized compounds accumulated in the bladder. The differentiation of clozapine concentrations within the rat brain was confirmed using a fast HPLC/MS/MS method. Close examination of the distribution of drugs within specific organs can also be used to assess drug penetration. Bouslimani *et al*. [161] showed that the platinum antitumor drug oxaliplatin was localized exclusively in the kidney cortex, suggesting that it did not penetrate deep into the organ.

The spatiochemical information provided by imaging MS has also been used to investigate the distribution of pharmaceutical compounds in tablet formulations [170]. Tablets are compacted pharmaceutical dosage forms that contain active drug compounds and excipients. These results indicate that imaging MS can assist in the development of drug-delivery systems as well as in lead development. MALDI imaging MS was recently exploited to independently measure the distribution of MRI contrast-enhancement agents in both frozen and paraformaldehyde-fixed mouse livers, which were independently validated by both an *in vivo* MRI and an *ex vivo* inductively coupled plasma atomic emission spectroscopy [171]. The development of targeted MRI contrast-enhancement agents is one of the key tools being developed for early, noninvasive detection of disease biomarkers, and imaging MS could provide an independent measurement of its distribution in tissue to ensure its colocalization with the target biomarker.

8.3.3.2 Endogenous Metabolites. Endogenous metabolites can give insight into metabolic changes linked to drug administration or disease. Among the endogenous

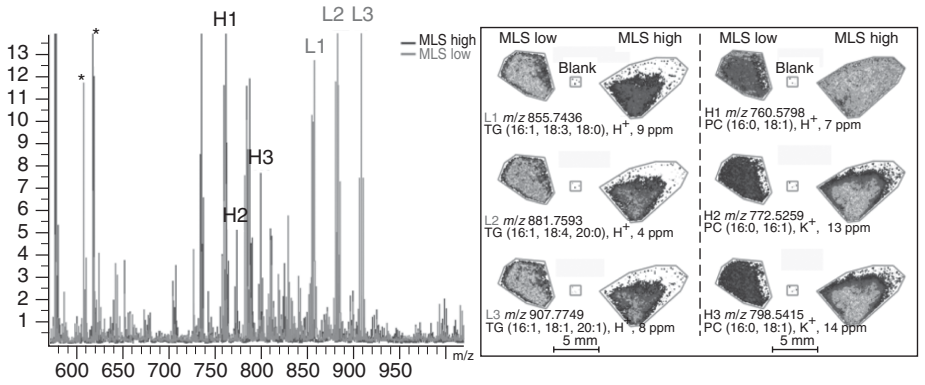

Figure 8.17 Lipid imaging mass spectrometry of high and low grade myxoid liposarcoma (MLS) reveals differential lipid profiles, and the spatial distributions show the localization of specific lipids in one tumor grade. The lipids were identified using tandem mass spectrometry. The experimental mass, the assignment, and the mass accuracy of the assignments are provided alongside the image [90]. *Matrix clusters. (See color insert.)

metabolites, simple lipids (e.g., cholesterol, acylglycerides, and fatty acids) and complex lipids (e.g., glycerophospholipids and glycosphingolipids), as well as aminoacids, flavonoids, and oligosaccharides, have been investigated and reviewed by Sugiura and Setou [154].

Lipid analysis of myxoid liposarcomas by imaging MS revealed differences between low and high grade tumors [90]. Low and high grade tumors each contain specifically expressed lipids whose images clearly reveal their localization to one grade (Fig. 8.17). These lipids were then identified using MS/MS and the LIPID MAPS database. The spectra from high grade tumors revealed higher levels of phosphocholines. Phosphocholines are commonly detected by MALDI and are thought to be derived from (cell) membranes. The higher levels of these lipids in high grade tumors are consistent with the higher cellularity of higher grade tumors [172]. Low grade myxoid liposarcoma contained additional peaks because of triacylglycerols. Active PPARγ signaling promotes adipocytic differentiation in preadipocytes and is active in myxoid liposarcoma cells [173]. The data suggest decreased PPARγ-regulated fatty acid synthesis in myxoid liposarcoma upon increase in grade, histologically reflected in a diminished adipocytic phenotype, and consistent with recent work that established that PPARγ inactivation by the FUS/DDIT3 liposarcoma-specific fusion protein is required for liposarcoma development [174].

The molecular ion distribution of intact lipids directly from single neuroblastoma cells was studied using matrix-enhanced (ME) SIMS. The ME-SIMS spectrum of these cell surfaces showed several lipid species in the mass range between m/z 700 and 900, ceramide, diacylglycerol species between m/z 500 and 700, and organic fragments in the lower mass range. High cholesterol signal intensity was found at the border of the cells, the plasma membrane, compared to the center of the cells, corresponding to the nuclei [175].

Background matrix peaks can be abundant in the low m/z range and can severely complicate metabolite imaging MS experiments. In order to improve the analysis of metabolites using imaging MS, different matrices have been investigated; 9-AA has

been reported as a highly promising matrix for metabolite analysis. No matrix signal was detected in the m/z range between 300 and 1000, the mass range where metabolite ion peaks are expected to be detected [64]. Furthermore, 13 primary metabolites at m/z values 323 (uridine monophosphate), 328 (cyclic adenosine monophosphate), 339 (fructose-1,6-biphosphate), 346 (adenosine monophosphate), 362 (guanosine monophosphate), 403 (uridine diphosphate), 426 (adenosine diphosphate), 442 (guanosine diphosphate), 506 (adenosine triphosphate), 522 (guanosine triphosphate), 558 (ADP-ribose), 565 (UDP-glucose), and 606 (UDP-GlcNAc) were observed, whereas none of them was detected using other matrices [64]. Identifications were made by tandem MS/MS comparing fragment fingerprints obtained from the tissue section and from standard samples. The distributions of those primary metabolites with a sensitivity of attomoles per pixel on rat brain sections were shown. As primary metabolites are known to be biomarkers of several brain disorders, imaging MS can be useful to study those metabolic changes [64].

8.4 PERSPECTIVES

Since its introduction in the late 1990s, MALDI imaging MS technology has made tremendous advances. Imaging MS is now used to investigate many different molecular classes, including peptides, proteins, lipids, metabolites, and drugs. The potential application of MALDI imaging MS in neurodegenerative diseases, cancer, viral infections, and drug metabolism lies in its ability to generate profiles in a nontargeted manner. These abilities enable the technique to detect unexpected and *a priori* unknown changes in the protein content of the tissue, for example, the presence of colorectal carcinoma biomarkers in histologically benign tissue [89], and to describe the tissue by a spectrum of peptides and proteins. MALDI imaging MS can also be adapted to span multiple molecular classes using essentially the same technique but different sample preparation strategies (peptides, proteins, lipids [118], and metabolites [64]), and can be integrated with established *in vitro* and *in vivo* analyses, thus the scope for complementary analyses is open. To investigate this potential in the clinic, the application largely driving the field, the biomolecular signatures obtained from the supervised and unsupervised analysis of the tissues are beginning to be tested across the large number of samples typically included in clinical cohorts [73].

To date, the classification of tissues using MALDI imaging MS has been based on established histological analysis [23,28,73]. The mass spectra obtained from a set of histologically annotated tissue sections are used to create a classifier, which is then applied to other tissue sections to test its performance. The ability of MALDI imaging MS to reproduce established histological classification demonstrates its ability to acquire clinically relevant data and can be considered the necessary first step of any new diagnostic/prognostic tool. The identification of new candidate protein profile biomarkers based on MALDI imaging MS, independent of histological analysis and thus able to detect biochemical changes before the appearance of pathological entities, has been performed for a small number of tissue sections [27,87]. Arguably, the next step in the development of MALDI-imaging-MS-based biomarker discovery is the development of classifiers based on the simultaneous analysis of tissue arrays. Such high throughput analysis will exploit the recently announced high speed MALDI mass spectrometers and imaging MS automation [98].

MALDI imaging MS is a rapidly developing tool that has great potential for improved diagnostic/prognostic capabilities. Nevertheless, it will be most effective when implemented as part of a concerted effort utilizing a range of complementary techniques and expertise.

MALDI imaging MS on small molecules has opened a new frontier both in pharmaceutical and toxicological research and in the developmental phase of new drugs. The potential of this technique lies in its ability to visualize and distinguish the parent drug and its metabolites and is an attractive alternative for monitoring drug distribution within animal models, with much faster results and lower cost than the traditional whole-body autoradiography method [85,176]. The possibility to monitor in parallel multiple analytes, with high specificity and rapid acquisition, makes it a very promising tool for drug development. Furthermore, this technique can study in one analysis the ability of the compound of interest to reach the target organ, the drug penetration into the target organ, and the diffusion to undesirable organs [161]. It offers the possibility of not only examining and tracking drug metabolism in whole animal sections but also following polymer substrate degradation and drug release.

REFERENCES

1. Coons AH, Creech HJ, Jones RN, *et al*. J Immunol 1942;45:159–170.
2. Hanash S. Nature 2003;422:226–232.
3. Portelius E, Zetterberg H, Gobom J, *et al*. Expert Rev Proteomics 2008;5:225–237.
4. Paradela A, Albar JP. J Proteome Res 2008;7:1809–1818.
5. Wepf A, Glatter T, Schmidt A, *et al*. Nat Methods 2009;6:203–205.
6. Han MH, Hwang SI, Roy DB, *et al*. Nature 2008;451:1076–1081.
7. Yan W, Aebersold R, Raines EW. J Proteomics 2009;72:4–11.
8. Sitek B, Sipos B, Alkatout I, *et al*. J Proteome Res 2009;8:1647–1656.
9. Chaurand P, Schwartz SA, Capriolo RM. Anal Chem 2004;76:87A–93A.
10. Chaurand P, Rahman MA, Hunt T, *et al*. Mol Cell Proteomics 2008;7:411–423.
11. Schwartz SA, Weil RJ, Johnson MD, *et al*. Clin Cancer Res 2004;10:981–987.
12. Cornett DS, Mobley JA, Dias EC, *et al*. Mol Cell Proteomics 2006;5:1975–1983.
13. Reyzer ML, Caldwell RL, Dugger TC, *et al*. Cancer Res 2004;64:9093–9100.
14. Rifai N, Gillette MA, Carr SA. Nat Biotechnol 2006;24:971–983.
15. Zabel C, Andreew A, Mao L, *et al*. Expert Rev Proteomics 2008;5:187–205.
16. Stoeckli M, Chaurand P, Hallahan DE, *et al*. Nat Med 2001;7:493–496.
17. Schwartz SA, Weil RJ, Thompson RC, *et al*. Cancer Res 2005;65:7674–7681.
18. Caprioli RM, Farmer TB, Gile J. Anal Chem 1997;69:4751–4760.
19. Crecelius AC, Cornett DS, Caprioli RM, *et al*. J Am Soc Mass Spectrom 2005; 16:1093–1099.
20. Pierson J, Norris JL, Aerni HR, *et al*. J Proteome Res 2004;3:289–295.
21. Stoeckli M, Staab D, Staufenbiel M, *et al*. Anal Biochem 2002;311:33–39.
22. Cornett DS, Reyzer ML, Chaurand P, *et al*. Nat Methods 2007;4:828–833.
23. Schwamborn K, Krieg RC, Reska M, *et al*. Int J Mol Med 2007;20:155–159.
24. Walch A, Rauser S, Deininger SO, *et al*. Histochem Cell Biol 2008;130:421–434.
25. McDonnell LA, van Remoortere A, van Zeijl RJ, *et al*. J Proteome Res 2008;7:3619–3627.
26. McCombie G, Staab D, Stoeckli M, *et al*. Anal Chem 2005;77:6118–6124.
27. Deininger SO, Ebert MP, Futterer A, *et al*. J Proteome Res 2008;7:5230–5236.
28. Groseclose MR, Massion PP, Chaurand P, *et al*. Proteomics 2008;8:3715–3724.
29. Oppenheimer SR, Mi D, Sanders ME, *et al*. J Proteome Res 2010;9:2182–2190.
30. Caldwell RL, Caprioli RM. Mol Cell Proteomics 2005;4:394–401.

31. Goodwin RJ, Dungworth JC, Cobb SR, *et al*. Proteomics 2008;8:3801–3808.
32. Schwartz SA, Reyzer ML, Caprioli RM. J Mass Spectrom 2003;38:699–708.
33. Amstalden van Hove ER, Smith DF, Heeren RM. J Chromatogr A 2010;1217:3946–3954.
34. Chughtai K, Heeren RM. Chem Rev 2010;110:3237–3277.
35. Kaletas BK, van der Wiel IM, Stauber J, *et al*. Proteomics 2009;9:2622–2633.
36. MacAleese L, Stauber J, Heeren RM. Proteomics 2009;9:819–834.
37. McDonnell LA, Heeren RM. Mass Spectrom Rev 2007;26:606–643.
38. Goodwin RJ, Pennington SR, Pitt AR. Proteomics 2008;8:3785–3800.
39. Lemaire R, Desmons A, Tabet JC, *et al*. J Proteome Res 2007;6:1295–1305.
40. Stauber J, Lemaire R, Franck J, *et al*. J Proteome Res 2008;7:969–978.
41. Fox CH, Johnson FB, Whiting J, *et al*. J Histochem Cytochem 1985;33:845–853.
42. Chaurand P, Latham JC, Lane KB, *et al*. J Proteome Res 2008;7:3543–3555.
43. Mange A, Chaurand P, Perrochia H, *et al*. J Proteome Res 2009;8:5619–5628.
44. Altelaar AF, Luxembourg SL, McDonnell LA, *et al*. Nat Protoc 2007;2:1185–1196.
45. Chaurand P, Norris JL, Cornett DS, *et al*. J Proteome Res 2006;5:2889–2900.
46. Chaurand P, Schwartz SA, Reyzer ML, *et al*. Toxicol Pathol 2005;33:92–101.
47. Lemaire R, Wisztorski M, Desmons A, *et al*. Anal Chem 2006;78:7145–7153.
48. Svensson M, Boren M, Skold K, *et al*. J Proteome Res 2009;8:974–981.
49. Goodwin RJ, Lang AM, Allingham H, *et al*. Proteomics 2010;10:1751–1761.
50. Seeley EH, Oppenheimer SR, Mi D, *et al*. J Am Soc Mass Spectrom 2008;19:1069–1077.
51. Ronci M, Bonanno E, Colantoni A, *et al*. Proteomics 2008;8:3702–3714.
52. Groseclose MR, Andersson M, Hardesty WM, *et al*. J Mass Spectrom 2007;42:254–262.
53. Gustafsson JO, Oehler MK, McColl SR, *et al*. J Proteome Res 2010;9:4315–4328.
54. Scholz B, Skold K, Kultima K, *et al*. Mol Cell Proteomics 2011;10:M900229–MCP200.
55. Grey AC, Chaurand P, Caprioli RM, *et al*. J Proteome Res 2009;8:3278–3283.
56. Leinweber BD, Tsaprailis G, Monks TJ, *et al*. J Am Soc Mass Spectrom 2009;20:89–95.
57. Franck J, Longuespee R, Wisztorski M, *et al*. Med Sci Monit 2010;16:BR293–BR299.
58. Karas M, Kruger R. Chem Rev 2003;103:427–440.
59. Wisztorski M, Lemaire R, Stauber J, *et al*. Curr Pharm Des 2007;13:3317–3324.
60. Wisztorski M, Croix D, Macagno E, *et al*. Dev Neurobiol 2008;68:845–858.
61. Fuchs B, Suss R, Schiller J. Prog Lipid Res 2010;49:450–475.
62. Bunch J, Clench MR, Richards DS. Rapid Commun Mass Spectrom 2004;18:3051–3060.
63. Nilsson A, Fehniger TE, Gustavsson L, *et al*. PLoS One 2010;5:e11411.
64. Benabdellah F, Touboul D, Brunelle A, *et al*. Anal Chem 2009;81:5557–5560.
65. Cheng H, Sun G, Yang K, *et al*. J Lipid Res 2010;51:1599–1609.
66. Luxembourg SL, McDonnell LA, Duursma MC, *et al*. Anal Chem 2003;75:2333–2341.
67. Hankin JA, Barkley RM, Murphy RC. J Am Soc Mass Spectrom 2007;18:1646–1652.
68. Puolitaival SM, Burnum KE, Cornett DS, *et al*. J Am Soc Mass Spectrom 2008; 19:882–886.
69. Trimpin S, Herath TN, Inutan ED, *et al*. Anal Chem 2010;82:359–367.
70. McDonnell LA, Corthals GL, Willems SM, *et al*. J Proteomics 2010;73:1921–1944.
71. Rompp A, Guenther S, Schober Y, *et al*. Angew Chem Int Ed Engl 2010;49:3834–3838.
72. Hardouin J. Mass Spectrom Rev 2007;26:672–682.
73. Cazares LH, Troyer D, Mendrinos S, *et al*. Clin Cancer Res 2009;15:5541–5551.
74. Djidja MC, Claude E, Snel MF, *et al*. J Proteome Res 2009;8:4876–4884.
75. Franck J, Ayed ME, Wisztorski M, *et al*. Methods Mol Biol 2010;656:323–338.
76. Chan K, Lanthier P, Liu X, *et al*. Anal Chim Acta 2009;639:57–61.
77. Guilhaus M, Selby D, Mlynski V. Mass Spectrom Rev 2000;19:65–107.
78. Stauber J, MacAleese L, Franck J, *et al*. J Am Soc Mass Spectrom 2010;21:338–347.
79. Taban IM, Altelaar AF, van der Burgt YE, *et al*. J Am Soc Mass Spectrom 2007;18:145–151.
80. Suckau D, Resemann A, Schuerenberg M, *et al*. Anal Bioanal Chem 2003;376:952–965.

81. van Remoortere A, van Zeijl RJ, van den Oever N, *et al*. J Am Soc Mass Spectrom 2010;21:1922–1929.
82. Hopfgartner G, Varesio E, Stoeckli M. Rapid Commun Mass Spectrom 2009;23:733–736.
83. Trim PJ, Djidja MC, Atkinson SJ, *et al*. Anal Bioanal Chem 2010;397:3409–3419.
84. Hsieh Y, Casale R, Fukuda E, *et al*. Rapid Commun Mass Spectrom 2006;20:965–972.
85. Stoeckli M, Staab D, Schweitzer A, *et al*. J Am Soc Mass Spectrom 2007;18:1921–1924.
86. Chaurand P, Schwartz SA, Billheimer D, *et al*. Anal Chem 2004;76:1145–1155.
87. Hanselmann M, Kothe U, Kirchner M, *et al*. J Proteome Res 2009;8:3558–3567.
88. Norris JL, Cornett DS, Mobley JA, *et al*. Int J Mass Spectrom 2007;260:212–221.
89. Pevsner PH, Melamed J, Remsen T, *et al*. Biomark Med 2009;3:55–69.
90. Willems SM, van Remoortere A, van Zeijl R, *et al*. J Pathol 2010;222:400–409.
91. van de Plas R, Ojeda F, Dewil M, *et al*. Pac Symp Biocomput 2007; 458–469.
92. McDonnell LA, van Remoortere A, de Velde N, *et al*. J Am Soc Mass Spectrom 2010;21:1969–1978.
93. Thiery G, Shchepinov MS, Southern EM, *et al*. Rapid Commun Mass Spectrom 2007;21:823–829.
94. Thiery G, Anselmi E, Audebourg A, *et al*. Proteomics 2008;8:3725–3734.
95. Lemaire R, Stauber J, Wisztorski M, *et al*. J Proteome Res 2007;6:2057–2067.
96. Monroe EB, Jurchen JC, Koszczuk BA, *et al*. Anal Chem 2006;78:6826–6832.
97. Zimmerman TA, Monroe EB, Sweedler JV. Proteomics 2008;8:3809–3815.
98. McDonnell LA, van Remoortere A, van Zeijl RJ, *et al*. J Proteomics 2010;73:1279–1282.
99. Chaurand P, Schwartz SA, Caprioli RM. J Proteome Res 2004;3:245–252.
100. Wehder L, Ernst G, Crecelius AC, *et al*. J Histochem Cytochem 2010;58:929–937.
101. Chaurand P, Sanders ME, Jensen RA, *et al*. Am J Pathol 2004;165:1057–1068.
102. Agar NY, Malcolm JG, Mohan V, *et al*. Anal Chem 2010;82:2621–2625.
103. Villanueva J, Philip J, DeNoyer L, *et al*. Nat Protoc 2007;2:588–602.
104. Andersson M, Groseclose MR, Deutch AY, *et al*. Nat Methods 2008;5:101–108.
105. Seeley EH, Caprioli RM. Proc Natl Acad Sci U S A 2008;105:18126–18131.
106. Sinha TK, Khatib-Shahidi S, Yankeelov TE, *et al*. Nat Methods 2008;5:57–59.
107. Iverson AA, Gillett C, Cane P, *et al*. J Mol Diagn 2009;11:117–130.
108. Rauser S, Marquardt C, Balluff B, *et al*. J Proteome Res 2010;9:1854–1863.
109. Djidja MC, Francese S, Loadman PM, *et al*. Proteomics 2009;9:2750–2763.
110. Seuma J, Bunch J, Cox A, *et al*. Proteomics 2008;8:3775–3784.
111. Callesen AK, Vach W, Jorgensen PE, *et al*. J Proteome Res 2008;7:1395–1402.
112. Yanagisawa K, Shyr Y, Xu BJ, *et al*. Lancet 2003;362:433–439.
113. Lemaire R, Menguellet SA, Stauber J, *et al*. J Proteome Res 2007;6:4127–4134.
114. Liu Y, Chen Y, Momin A, *et al*. Mol Cancer 2010;9:186.
115. Kean EL. J Lipid Res 1968;9:319–327.
116. Cazares LH, Adam BL, Ward MD, *et al*. Clin Cancer Res 2002;8:2541–2552.
117. Djidja MC, Claude E, Snel MF, *et al*. Anal Bioanal Chem 2010;397:587–601.
118. Shimma S, Sugiura Y, Hayasaka T, *et al*. J Chromatogr B Anal Technol Biomed Life Sci 2007;855:98–103.
119. Kim HK, Reyzer ML, Choi IJ, *et al*. J Proteome Res 2010;9:4123–4130.
120. Looser KG, Shah JP, Strong EW. Head Neck Surg 1978;1:107–111.
121. Caldwell RL, Gonzalez A, Oppenheimer SR, *et al*. Cancer Genomics Proteomics 2006;3:279–287.
122. Predki PF, Mattoon D, Bangham R, *et al*. Hum Antibodies 2005;14:7–15.
123. Caldwell RL, Opalenik SR, Davidson JM, *et al*. Wound Repair Regen 2008;16:442–449.
124. Kang S, Shim HS, Lee JS, *et al*. J Proteome Res 2010;9:1157–1164.
125. Mentzel T, Calonje E, Wadden C, *et al*. Am J Surg Pathol 1996;20:391–405.
126. Marusyk A, Polyak K. Biochim Biophys Acta 2010;1805:105–117.
127. Campbell LL, Polyak K. Cell Cycle 2007;6:2332–2338.

128. Mentzel T. J Pathol 2000;190:523–525.
129. Beerman H, Smit VT, Kluin PM, *et al*. Cytometry 1991;12:147–154.
130. Bonsing BA, Corver WE, Fleuren GJ, *et al*. Genes Chromosomes Cancer 2000; 28:173–183.
131. Jespersen S, Chaurand P, van Strien FJ, *et al*. Anal Chem 1999;71:660–666.
132. Jackson SN, Wang HY, Woods AS, *et al*. J Am Soc Mass Spectrom 2005;16:133–138.
133. Jackson SN, Wang HY, Woods AS. Anal Chem 2005;77:4523–4527.
134. Jackson SN, Wang HY, Woods AS. J Am Soc Mass Spectrom 2005;16:2052–2056.
135. Jackson SN, Wang HY, Woods AS. J Am Soc Mass Spectrom 2007;18:17–26.
136. Jackson SN, Ugarov M, Egan T, *et al*. J Mass Spectrom 2007;42:1093–1098.
137. Jackson SN, Woods AS. J Chromatogr B Anal Technol Biomed Life Sci 2009; 877:2822–2829.
138. Mikawa S, Suzuki M, Fujimoto C, *et al*. Neurosci Lett 2009;451:45–49.
139. Langstrom B, Andren PE, Lindhe O, *et al*. Mol Imaging Biol 2007;9:161–175.
140. Basso M, Giraudo S, Corpillo D, *et al*. Proteomics 2004;4:3943–3952.
141. Stoeckli M, Knochenmuss R, McCombie G, *et al*. Methods Enzymol 2006;412:94–106.
142. Yao I, Sugiura Y, Matsumoto M, *et al*. Proteomics 2008;8:3692–3701.
143. Kunze D, Reichmann G, Egger E, *et al*. Eur J Clin Invest 1975;5:471–475.
144. Rando TA, Disatnik MH, Yu Y, *et al*. Neuromuscul Disord 1998;8:14–21.
145. Touboul D, Piednoel H, Voisin V, *et al*. Eur J Mass Spectrom (Chichester, Eng) 2004;10:657–664.
146. Touboul D, Brunelle A, Halgand F, *et al*. J Lipid Res 2005;46:1388–1395.
147. Tahallah N, Brunelle A, De La Porte S, *et al*. J Lipid Res 2008;49:438–454.
148. Grey AC, Schey KL. Mol Vis 2008;14:171–179.
149. Grey AC, Schey KL. Invest Ophthalmol Vis Sci 2009;50:4319–4329.
150. Han J, Schey KL. Invest Ophthalmol Vis Sci 2006;47:2990–2996.
151. Thibault DB, Gillam CJ, Grey AC, *et al*. J Am Soc Mass Spectrom 2008;19:814–822.
152. Vidova V, Pol J, Volny M, *et al*. J Lipid Res 2010;51:2295–2302.
153. Reyzer ML, Hsieh Y, Ng K, *et al*. J Mass Spectrom 2003;38:1081–1092.
154. Sugiura Y, Setou M. J Neuroimmune Pharmacol 2010;5:31–43.
155. Cornett DS, Frappier SL, Caprioli RM. Anal Chem 2008;80:5648–5653.
156. Khatib-Shahidi S, Andersson M, Herman JL, *et al*. Anal Chem 2006;78:6448–6456.
157. Rohner TC, Staab D, Stoeckli M. Mech Ageing Dev 2005;126:177–185.
158. Garrett TJ, Yost RA. Anal Chem 2006;78:2465–2469.
159. Shimma S, Sugiura Y, Hayasaka T, *et al*. Anal Chem 2008;80:878–885.
160. Trim PJ, Henson CM, Avery JL, *et al*. Anal Chem 2008;80:8628–8634.
161. Bouslimani A, Bec N, Glueckmann M, *et al*. Rapid Commun Mass Spectrom 2010;24:415–421.
162. Atkinson SJ, Loadman PM, Sutton C, *et al*. Rapid Commun Mass Spectrom 2007;21:1271–1276.
163. Vegvari A, Fehniger TE, Gustavsson L, *et al*. J Proteomics 2010;73:1270–1278.
164. Dekker LJ, van Kampen JJ, Reedijk ML, *et al*. Rapid Commun Mass Spectrom 2009;23:1183–1188.
165. Reyzer ML, Caprioli RM. Curr Opin Chem Biol 2007;11:29–35.
166. Taira S, Sugiura Y, Moritake S, *et al*. Anal Chem 2008;80:4761–4766.
167. Liu Q, Xiao Y, Pagan-Miranda C, *et al*. J Am Soc Mass Spectrom 2009;20:80–88.
168. Liu Q, Guo Z, He L. Anal Chem 2007;79:3535–3541.
169. Northen TR, Yanes O, Northen MT, *et al*. Nature 2007;449:1033–1036.
170. Earnshaw CJ, Carolan VA, Richards DS, *et al*. Rapid Commun Mass Spectrom 2010;24:1665–1672.
171. Acquadro E, Cabella C, Ghiani S, *et al*. Anal Chem 2009;81:2779–2784.
172. Bensinger SJ, Tontonoz P. Nature 2008;454:470–477.

173. Tontonoz P, Spiegelman BM. Annu Rev Biochem 2008;77:289–312.
174. Perez-Mancera PA, Vicente-Duenas C, Gonzalez-Herrero I, *et al*. Carcinogenesis 2007;28:2069–2073.
175. Altelaar AF, Piersma SR. Methods Mol Biol 2010;656:197–208.
176. Anderson L, Hunter CL. Mol Cell Proteomics 2006;5:573–588.